Noise-Enhanced Detection of Subthreshold Signals With Carbon Nanotubes

Ian Lee, Xiaolei Liu, Chongwu Zhou, and Bart Kosko, *Member, IEEE*

***Abstract*—Electrical noise can help pulse-train signal detection at the nanolevel. Experiments on a single-walled carbon nanotube transistor confirmed that a threshold exhibited stochastic resonance (SR) for finite-variance and infinite-variance noise: small amounts of noise enhanced the nanotube detector's performance. The experiments used a carbon nanotube field-effect transistor to detect noisy subthreshold electrical signals. Two new SR hypothesis tests in the Appendix also confirmed the SR effect in the nanotube transistor. Three measures of detector performance showed the SR effect: Shannon's mutual information, the normalized correlation measure, and an inverted bit error rate compared the input and output discrete-time random sequences. The nanotube detector had a threshold-like input–output characteristic in its gate effect. It produced little current for subthreshold digital input voltages that fed the transistor's gate. Three types of *synchronized* white noise corrupted the subthreshold Bernoulli sequences that fed the detector. The Gaussian, the uniform, and the impulsive Cauchy noise combined with the random input voltage sequences to help the detector produce random output current sequences. The experiments observed the SR effect by measuring how well an output sequence matched its input sequence. Shannon's mutual information used histograms to estimate the probability densities and computed the entropies. The correlation measure was a scalar inner product of the input and output sequences. The inverted bit error rate computed how often the bits matched between the input and output sequences. The observed nanotube SR effect was robust: it persisted even when infinite-variance Cauchy noise corrupted the signal stream. Such noise-enhanced signal processing at the nanolevel promises applications to signal detection in wideband communication systems and biological and artificial neural networks.**

***Index Terms*—Antenna arrays, carbon nanotube field-effect transistors (FETs), communication systems, correlation, detectors, infinite-variance noise, Kolmogorov–Smirnov statistics, nanotechnology, noise processing, signal processing, stochastic resonance (SR) hypothesis tests, stochastic processes, stochastic resonance (SR), threshold detection.**

I. Introduction

NOISE CAN sometimes help neurons and other nonlinear systems detect signals. Several researchers have demonstrated the stochastic resonance (SR) effect for various types of threshold units or neurons [1]–[11]. Fig. 1 shows how additive white uniform pixel noise can improve the quality of the degraded image of a carbon nanotube. We produced these noisy images by applying a pixel-level threshold to an artistic rendering of a carbon nanotube. The threshold gives a white pixel $y = 1$ as output if the input grayscale pixel $x \in [0, 1]$ equals or exceeds a threshold θ: $y = g(x+n-\theta) = 1$ for $(x+n-\theta) \geq 0$ and $y = 0$ for $(x + n - \theta) < 0$.

The new SR theorems in [1] give broad sufficient conditions for SR to occur in any threshold system for all possible finite-variance noise types and for most infinite-variance noise types. We restate these SR theorems below. Simulations show that these SR theorems apply to a threshold-like ramp function that often models a transistor's current–voltage $(I–V_G)$ characteristics: $Y = G(S - V_T)$ where Y is the output current, V_T is the threshold voltage, and G is a nonzero gain for suprathreshold inputs $S \geq V_T$ and zero otherwise.

Fig. 1(e) shows the signature SR curves for a simulated transistor that had parameters $G = -1$ nA/V and $V_T = -2$ V based on a nanotube transistor and for Shannon's mutual information $I(S, Y)$, a normalized correlation measure $C(S, Y)$, and an inverted bit error rate $1-$BER. The SR curves have similar optimal noise standard deviations σ_{opt} in the interval (0.3,0.5). The vertical dashed lines show the maximal and minimal ranges of 100 trials. Each trial produced 10 000 input–output pairs (s_i, y_i). The input $s_i = b_i + n_i$ was a sum of Gaussian noise n_i and binary input (Bernoulli) symbols b_i for the equally likely ON/OFF symbol pair -1.6 V and -1.4 V. These simulations led to the natural prediction that an actual nanotube transistor would exhibit the SR effect.

Experiments observed that three types of noise helped a carbon nanotube transistor detect subthreshold signals and confirmed the SR prediction using three performance measures and two statistical tests. Section II summarizes the noisy nanotube experimental findings that demonstrated the SR effect at the nanoscale. Section III reviews nanotube transistors and stochastic-resonance theory. Section IV provides a detailed description of the experimental setup and results.

II. Noise-Enhanced Nano Signal Detection

Experiments confirmed the SR prediction: noise helped a pristine (undoped) single-walled carbon nanotube transistor [12]–[17] detect subthreshold signals. The experiments applied different Bernoulli input sequences that used different combinations of subthreshold gate voltages as their ON/OFF symbols. *Synchronized* Gaussian, uniform, and infinite-variance Cauchy noise added to the input sequences and helped the nanotube transistor detect the subthreshold input. The performance measures were Shannon's mutual information $I(S, Y)$, an input–output correlation measure $C(S, Y)$, and an inverted bit error rate $1 -$ BER.

Manuscript received January 26, 2004; revised July 7, 2006. This work was supported in part by the National Science Foundation under Grant ECS-0070284. The review of this paper was arranged by Associate Editor D. Frank.

The authors are with the Department of Electrical Engineering, University of Southern California, Los Angeles, CA 90089-2564 USA (e-mail: kosko@usc.edu).

Color versions of Figs. 1–3 and 5–10 are available online at http://ieeexplore.ieee.org.

Digital Object Identifier 10.1109/TNANO.2006.883476

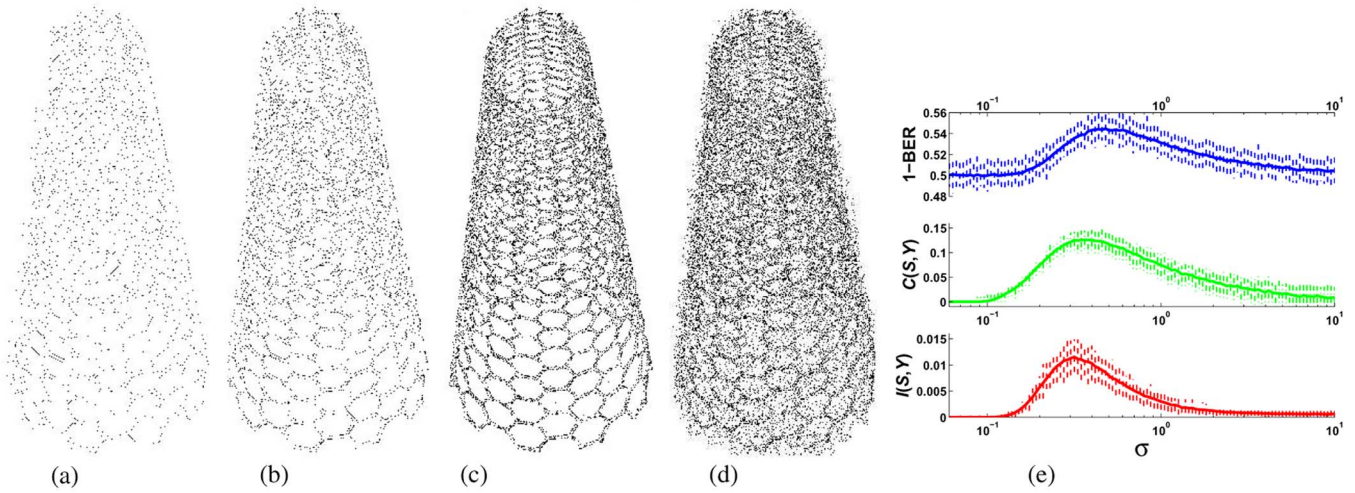

Fig. 1. Uniform pixel noise can improve the quality of an image through a stochastic-resonance effect. (a) The faint image results when we apply the threshold $\theta = 0.001$ to the original image. Figures (b) through (d) show the effect of increasing additive noise uniformly distributed over $(-A, A)$. (e) The simulation clipped the noisy input s_i to fit the range $[-5, 5]$ V to match an experimental limit. Both the mutual information and the inverted bit error rate applied a minimum-distance two-class discriminant function to classify the output data into a binary sequence of zeros and ones.

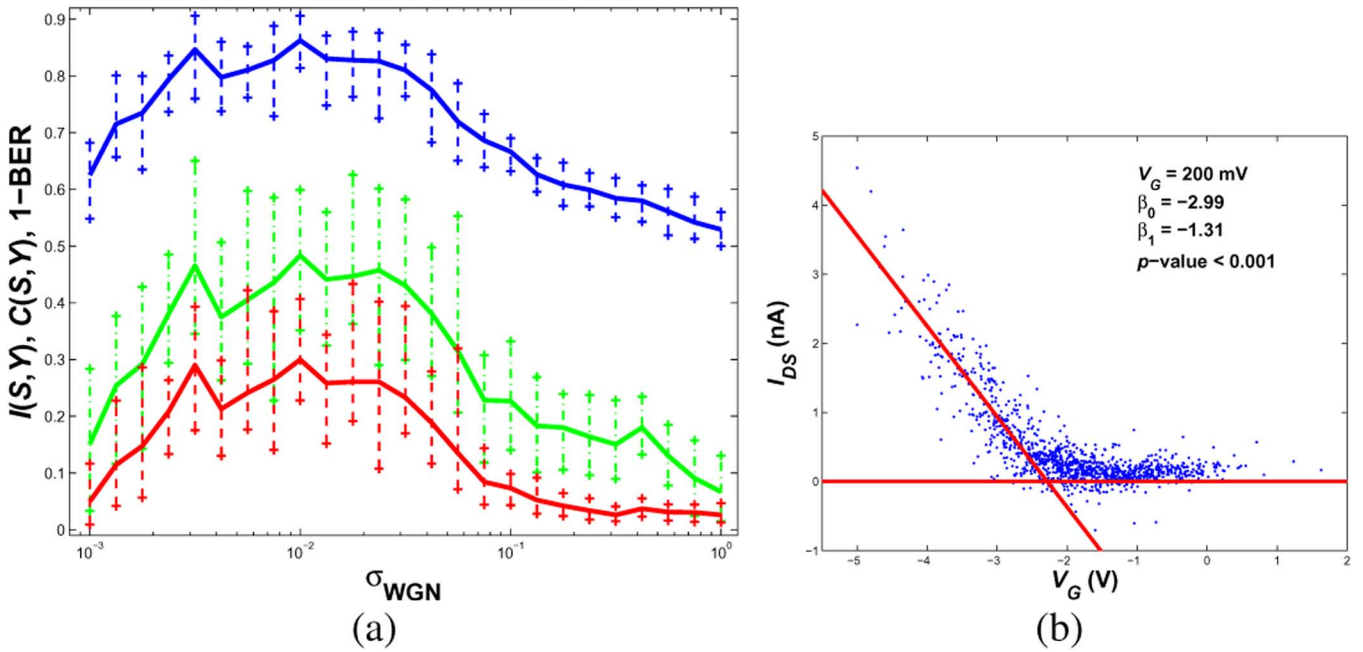

Fig. 2. Nanotube threshold detector exhibits SR. (a) Detection performance gave the nonmonotonic SR signature with similar modes for a nanotube transistor and for additive white Gaussian noise. The three performance measures were the bottom red mutual-information curve $I(S, Y)$, the middle green correlation-measure curve $C(S, Y)$, and the top blue inverted bit-error-rate curve $1 - \text{BER}$ that varied with the standard deviation σ of the Gaussian noise. (b) The stochastic I-V_G curve shows a threshold-like gate effect of the p-type nanotube detector. Linear regression of the random input–output pair (s_i, y_i) estimated the threshold gate voltage $V_T = -2.3$ V.

Fig. 2(a) shows the nonmonotonic signature of SR for white Gaussian noise. The three SR curves had similar modes that occurred for nonzero noise strength with a standard deviation of at least 0.01. Each vertical dashed bar occurs at one of the 25 sampled noise values and shows the maximal and minimal range of 32 averaged experimental trials. Each trial applied 1000 subthreshold symbols to the detector. The solid polygonal line connects the means of those 25 sets of experiments to form the SR curves.

Both the simulated and experimental nanotube detector had correlated SR curves. The correlation coefficient R measured the strength of the correlation. The simulated SR curves had correlation coefficients of $R = 0.9367$ for $I(S, Y)$ and $C(S, Y)$, $R = 0.8265$ for $I(S, Y)$ and $1 - \text{BER}$, and $R = 0.9541$ for $C(S, Y)$ and $1 - \text{BER}$. The experimental SR curves had correlation coefficients of $R = 0.9830$ for $I(S, Y)$ and $C(S, Y)$, $R = 0.9774$ for $I(S, Y)$ and $1 - \text{BER}$, and $R = 0.9877$ for $C(S, Y)$ and $1 - \text{BER}$. The correlations were statistically significant for p-value < 0.001.

The SR curves were nonmonotonic: a χ^2-test and a Kolmogorov–Smirnov test both rejected the similarity between a monotonically decreasing β-probability density function and each of the three SR curves with p-value < 0.001. Nonlinear stochastic experiments can have extreme variations (vertical bars). Both the simulated and experimental SR curves have similar variations that can be as much as half the height of the SR modes.

We observed the nanotube SR effect in Fig. 2(a) as one of four such successful combinations of input binary values with the parameter choices ON $= -1.6$ V and OFF $= -1.4$ V. This SR effect occurred despite the nanotube instabilities that caused fluctuations in the stochastic I-V_G curve in Fig. 2(b). The plot shows the threshold-like nonlinearity of the nanotube transistor that differed from the hysteretic loops in Fig. 4 that the nanotube detector exhibited and differed from the hysteretic loops in [18]. Fig. 2(b) plots the experimental input–output pairs (s_i, y_i) and shows the transistor's current–voltage I–V_G characteristics in response to noisy input signals. Linear regression fit the data to the transistor equation, extrapolated the nonlinearity in Fig. 2(b), and estimated the threshold voltage $\hat{V_T} \approx -2.3$ V.

The nanotube experiments produced the SR effect for Shannon's mutual information [19], an input–output correlation measure [20], [21], and an inverted bit error rate that measured how well the output sequences matched the input Bernoulli sequences. The mutual information $I(S,Y)$ subtracts the noisy channel's (the transistor's) output conditional entropy $H(Y|S)$ from its unconditional entropy $H(Y)$: $I(S,Y) = H(Y) - H(Y|S)$ [22]. The input signal S was a sequence of random binary voltages that produced a random output sequence Y in the form of a transistor current. Histograms of the sequences estimated the probability density functions that computed the entropies. The correlation measure $C(S,Y)$ normalized the zero-lag value of the cross-correlation sequence

$$r_{SY}(l) = \sum_{k=1}^{N} s(k)y(k-l) \tag{1}$$

of the two sequences with subtracted means. These two measures did not assume that the nanotube detector had a special structure and did not impose a threshold scheme on the experiment. But the inverted bit error rate $(1 - \text{BER})$ decided whether each output y_i was a '0' or '1' by applying a threshold scheme: a Bayes discriminant function in a two-class minimum-distance classifier [23] that used complete knowledge of the input. The $1 - \text{BER}$ measured how often the input and output bits agreed: $1 - \text{BER} = 1 - (N_{\text{error}}/N) = N_{\text{correct}}/N$ where N_{error} counted the number of bits that differed between the length-N input and output sequences and N_{correct} counted the number of bits that agreed.

III. Background

A. Carbon Nanotube Field Effect Transistors

A semiconductor single-walled carbon nanotube (SWNT) can change its conductivity in response to an external electric field in a gate effect [12], [14]. The SR experiments used a chemical-vapor-deposition (CVD) grown SWNT [24]–[27]. The semiconductor SWNT forms a Schottky diode at the interface with metal so that a metal-nanotube-metal contact forms a field-effect transistor (FET) with an adjacent gate electrode [28]. The typical current–voltage $(I$–$V_G)$ characteristics

$$I = \begin{cases} G(V - V_T) & \text{for } V_G \le V_T \\ 0 & \text{else} \end{cases} \tag{2}$$

indicate that the pristine semiconductor nanotubes act as hole-doped semiconductors at room temperatures and that the nanotube devices are p-type FETs [12]–[14], [29]. The transconductance G is negative and the gate voltage $V_G \le V_T$ is suprathreshold for p-type FETs.

The SR theoretical result does not specify the material or the dimensions of the threshold device. So the theory could apply to non–carbon nanotube transistors. Non–carbon nanotube materials such as inorganic nanotubes, nanowires, and nanofibers can act as the conduction channel in nanoscale transistors [33], [42]. Such non–carbon nanotube devices have the threshold-like characteristics that satisfy the SR theory.

B. Stochastic Resonance

SR occurs when noise enhances the performance of a nonlinear system [9]. The SR effect occurs in nature, in electrical systems, in neuron models, and in climate [7], [43]–[92] but no report of SR in carbon nanotubes. The SR effect can also exhibit more than one mode [93]–[95]. Examples of neuronal models that exhibit the SR effect include dynamical models [10], [20], [21], [96]–[105] and threshold units or neurons [19]–[21], [48], [106]–[108] for finite-variance noise types and using mutual information or cross-correlation to measure the performance.

[1] shows that a simple threshold is a sufficient condition for the SR effect and for all finite-variance noise and for all major infinite-variance noise. We review two theorems from [1]; they show that small amounts of independent additive noise can increase the mutual information of threshold neurons if the neurons detect subthreshold noisy Bernoulli input signals. The first theorem shows that the SR effect occurs for all finite-variance noise probability density functions (pdf) that obey a simple mean constraint. The second theorem shows that the SR effect holds for all infinite-variance noise types in the broad family of stable distributions.

The theorems use the standard discrete-time threshold neuron model [1] (and references therein).

$$y = \text{sgn}(s + n - \theta) = \begin{cases} 1 & \text{if } s + n \ge \theta \\ 0 & \text{if } s + n < \theta \end{cases} \tag{3}$$

where $\theta > 0$ is the neuron's threshold, s is the bipolar input Bernoulli signal with arbitrary success probability p such that $0 < p < 1$ and with amplitude $A > 0$, and n is the additive white noise with probability density $p(n)$.

The threshold neuron study uses binary signals that have subthreshold symbols. The symbol '0' denotes the input signal $s = -A$ and output signal $y = 0$. The symbol '1' denotes input signal $s = A$ and output signal $y = 1$. We assume subthreshold input signals: $A < \theta$. Then the conditional probabilities $P_{Y|S}(y|s)$ are

$$\begin{aligned} P_{Y|S}(0|0) &= \Pr\{s + n < \theta\}|_{s=-A} = \Pr\{n < \theta + A\} \\ &= \int_{-\infty}^{\theta+A} p(n)dn \end{aligned} \tag{4}$$

$$P_{Y|S}(1|0) = 1 - P_{Y|S}(0|0) \tag{5}$$

$$\begin{aligned} P_{Y|S}(0|1) &= \Pr\{s + n < \theta\}|_{s=A} = \Pr\{n < \theta - A\} \\ &= \int_{-\infty}^{\theta-A} p(n)dn \end{aligned} \tag{6}$$

$$P_{Y|S}(1|\,1) = 1 - P_{Y|S}(0|1) \tag{7}$$

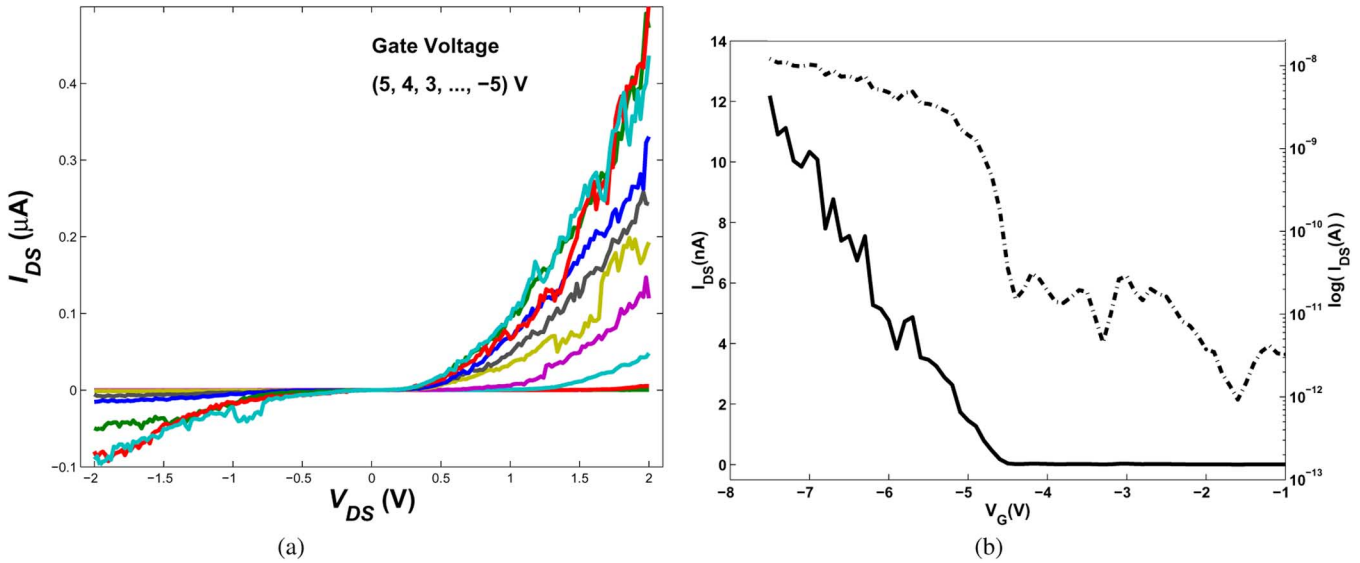

Fig. 3. Nanotube transistor changes its conductance in a gate effect. (a) I-V_D curves plot the transistor current I as a function of drain–source voltage $V_{\rm DS}$. (b) The nanotube transistor's current–voltage curves show a nonlinear gate effect. The figure plots current I as a function of gate voltage V_G. The upper dash-dot line is the log-scale I-V_G curve. The drain–source voltage $V_{\rm DS}$ was 200 mV.

and the marginal density is

$$P_Y(y) = \sum_S P_{Y|S}(y|s)P_S(s). \tag{8}$$

The performance measure is Shannon's mutual information. The discrete mutual information of the input S and output Y is the difference between the output unconditional entropy $H(Y)$ and the output conditional entropy $H(Y|S)$ conditioned on the input

$$I(S,Y) = H(Y) - H(Y|S) \tag{9}$$

$$= \sum_s \sum_y P_{SY}(s,y) \log \frac{P_{SY}(s,y)}{P_S(s)P_Y(y)}. \tag{10}$$

So the mutual information is the expectation of the random variable $\log[P_{SY}(s,y)/P_S(s)P_Y(y)]$:

$$I(S,Y) = E\left[\log \frac{P_{SY}(s,y)}{P_S(s)P_Y(y)}\right]. \tag{11}$$

Here $P_S(s)$ is the probability density of the input S, $P_Y(y)$ is the probability density of the output Y, $P_{Y|S}(y|s)$ is the conditional density of the output Y given the input S, and $P_{SY}(s,y)$ is the joint density of the input S and the output Y. Simple bipolar histograms of samples can estimate these densities in practice. The mutual information is the relative entropy between the joint density $P_{SY}(s,y)$ and the product density $P_S(s)P_Y(y)$. We note that the mutual information is zero if S and Y are independent and give $\log(1) = 0$ in (11): the joint density is the product of the marginal densities $P_{SY}(s,y) = P_S(s)P_Y(y)$. Jensen's inequality [22] implies that the mutual information is nonnegative: $I(S,Y) \geq 0$.

Theorem 1: Suppose that the threshold neuron (3) has noise probability density function $p(n)$ and that the input signal S is subthreshold $(A < \theta)$. Suppose that there is some statistical dependence between the input random variable S and output random variable Y (so that $I(S;Y) > 0$). Suppose that the noise mean $E[n]$ does not lie in the signal-threshold interval $(\theta - A, \theta + A)$ if $p(n)$ has finite variance. Then the threshold neuron (3) exhibits the nonmonotone SR effect in the sense that $I(S,Y) \to 0$ as $\sigma \to 0$.

Theorem 2: Suppose $I(S,Y) > 0$ and the threshold neuron (3) uses α-stable noise with location parameter $a \notin (\theta - A, \theta + A)$. Then the neuron (3) exhibits the nonmonotone SR effect if the input signal is subthreshold.

IV. Experimental Observation of Nanotube SR

The nanotube experiments confirmed the SR prediction [1] for a nanometer-wide transistor detecting noisy Bernoulli signals and for both finite-variance and infinite-variance noise. The nanotube detector exhibited the SR effect by comparing the random Bernoulli input signal to the random output and computing Shannon's mutual information, the normalized correlation measure, and the inverted bit error rate. Each of the nanotube experiments applied 25 sampled noise levels that ranged from 0.001 to 1 standard deviation σ (dispersion γ for infinite-variance Cauchy) linearly in logarithmic scale. The noisy input S was a *synchronized* Bernoulli sequence $s_i = b_i + n_i$ of the sum of random subthreshold binary values b_i and additive white noise n_i of three types. So there was no *timing* noise in the pulse train as in the FHN neuron model [10], [11]. Synchronization allows the nanotube systems to implement a variety of algorithms from signal processing and communications. The experiments updated the noisy input symbols s_i about once every 10 ms. A 200-mV drain–source voltage biased the nanotube at room temperature in vacuum. The experiments measured and averaged ten samples of the detector output at 100 kilosamples/s near the end of each symbol interval to estimate the output symbols y_i.

A. Materials and Methods

The experiments tested a carbon nanotube FET as a threshold detector with subthreshold signal plus noise. The detector consisted of a single-walled semiconductor carbon nanotube bridging two electrodes. [26] contains details of the fabrication. A voltage is subthreshold if it is more positive than a p-type

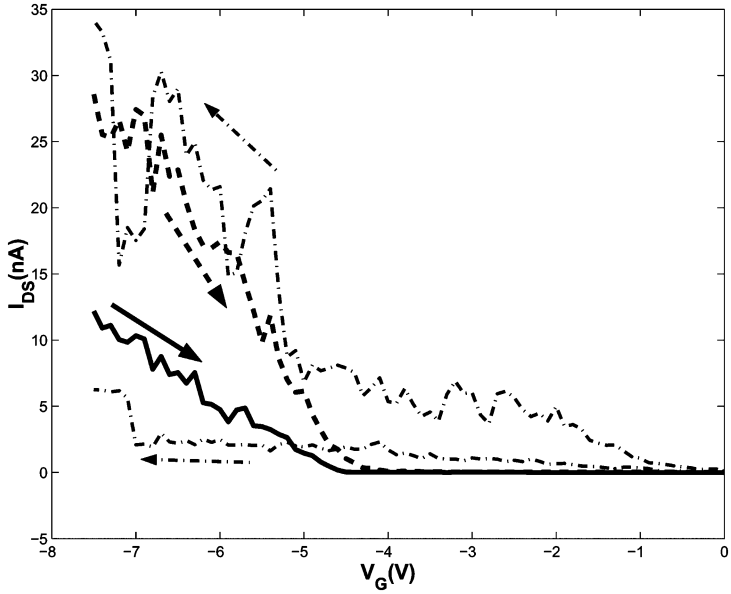

Fig. 4. Transistor I–V_G curves show two hysteretic loops. The hysteresis changes after exposure to vacuum. The upper pair shows the atmospheric hysteretic loop. The arrows in the plot show the directions of the voltage sweeps. Thin dash-dot lines are for sweeps to the left and the thicker lines (dash on top and solid on bottom) are for sweeps to the right.

FET's threshold voltage and produces picoamp current in an OFF state. The experiment tested whether noise could enhance subthreshold signals to produce measurable currents.

The CVD technique combined with e-beam lithography to grow a single-walled nanotube that was 3–5 μm long and less than 2 nm in diameter between two electrodes. The gap between the electrodes was approximately 3 μm wide but the single-walled nanotube was not straight as it spanned the gap. Atomic force microscopy examined the detector and showed that the nanotube had a diameter $d < 2$ nm that was consistent with a single-walled nanotube.

Four steps prepared the nanotube detector: screening, wafer cutting, wire bonding, and vacuum pumping. The pumping step held a detector and its carrier in a cryostat while a vacuum pump evacuated air and contaminants such as water. The experiments tested the nanotube at room temperature and used the cryostat to control the detector's environment.

A Hewlett-Packard 4156B Semiconductor Parameter Analyzer characterized the transistor behavior in the current–voltage plots in Fig. 3. The analyzer used dc voltages in gradual steps: it varied the drain–source voltage V_D from -2 to 2 V while keeping the gate voltage V_G constant to produce I–V_D curves. Each curve corresponds to a different $V_G \in \{-5, -4, -3, \ldots, 4, 5\}$ V in Fig. 3(a). The analyzer stepped the gate voltage V_G from -7.5 to 7.5 V in a single sweep and kept V_D was constant at 200 mV to produce I-V_G curves in Fig. 3(b).

Fig. 2(b) plotted the detector's output current Y against the input voltage S and showed the p-type transistor behavior of the detector with little hysteresis. Linear regression estimated the transconductance and the threshold voltage. The estimated threshold voltage is where the regression line intersects the bottom axis. These estimated parameters differed from those of the I-V_G curve that the semiconductor analyzer produced in Fig. 3(b). The hysteretic effect could account for the differences: different parts of the hysteretic loop gave different parameters for the gate effect. The experiments used input voltages that changed magnitudes at random and produced data in Fig. 2(b) that averaged the hysteretic effect.

A PC-based National Instruments PCI-MI0-16XE-10 data acquisition (DAQ) board converted the noise-corrupted signal S from digital to analog (DA) and converted the conditioned noisy output Y from analog to digital (AD). The AD–DA conversion has a 16-bit resolution and a 10-(μs) rise time. The DAQ board has a selected input voltage range in the interval $[-5, 5]$ V for AD conversion and a fixed output voltage range in the interval $[-10, 10]$ V for DA conversion. A voltage divider divided the output voltage by two and improved the resolution of the DAQ's analog output voltage.

A DL 1211 current–voltage preamplifier conditioned the detector output current Y before data acquisition sampled it as a voltage. The amplifier converts a small current (10 nA) into a large voltage (1 V) with the 10^{-8} A/V gain setting. The analog voltage has a maximal time delay of 0.1 ms with the 0.1-ms rise-time setting. A software driver in LabView produced the random signal S and the additive noise. The program also timed the update of the noisy signal sequence and supervised the DA and AD conversions.

B. Nanotube SR Experimental Results

The experiments found the SR effect for mutual information, normalized correlation, and inverted bit error rate for Gaussian (Fig. 5) and uniform (Fig. 6) noise and for four combinations of binary symbols (a) $(-2.0, -1.8)$ V, (b) $(-1.8, -1.6)$ V, (c) $(-1.6, -1.4)$ V, and (d) $(-1.4, -1.2)$ V. Each pair had a 0.2-V separation because sensitivity analysis showed that the separation gave complete SR modes within the range of noise levels. A linear regression of the transistor's gate effect estimated the threshold voltage and aided the selection of the subthreshold ON/OFF symbols.

Fig. 5 shows that the SR mode or optimal noise level σ_{opt} was the same standard deviation value between 0.01 and 0.1 for (a)

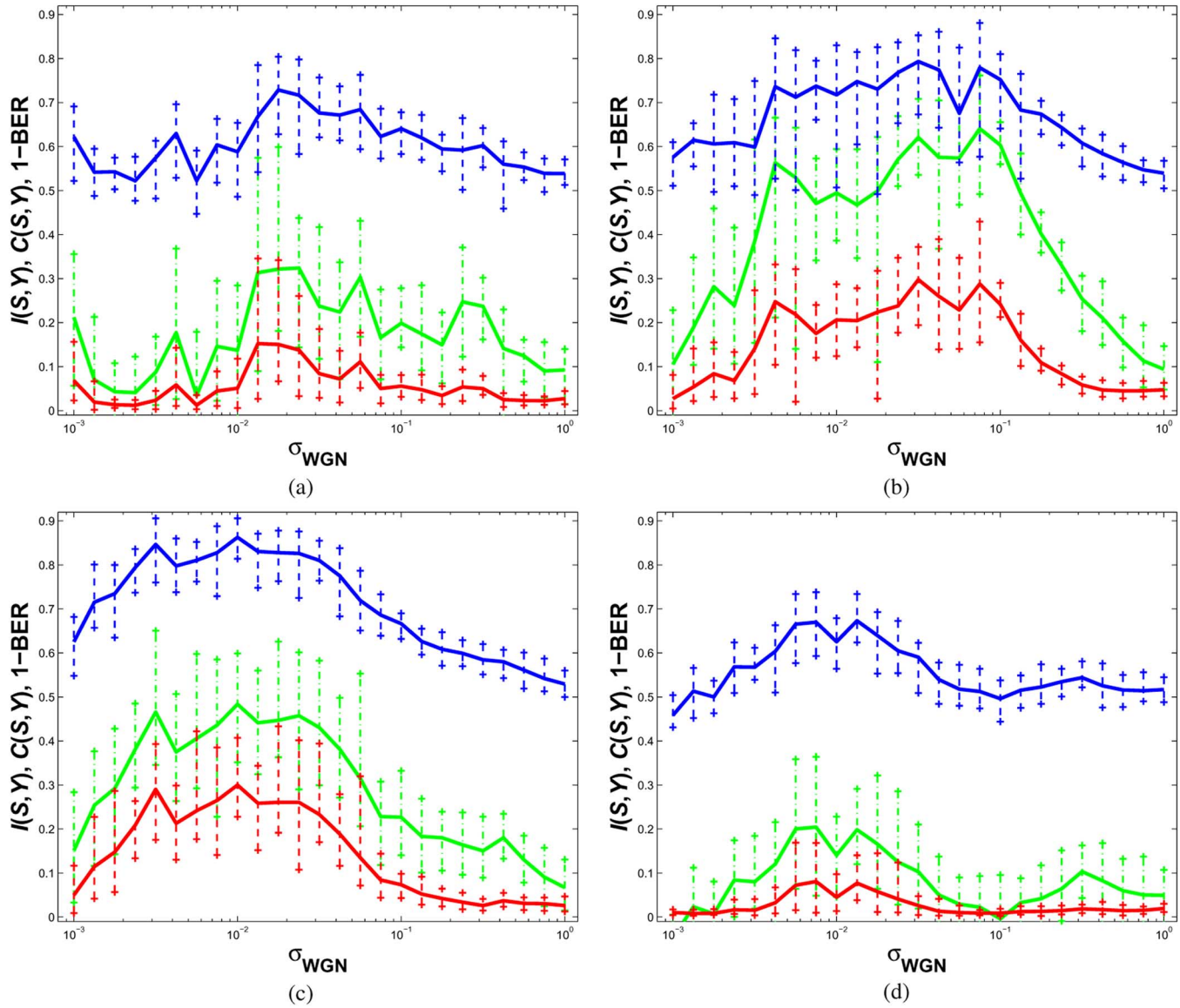

Fig. 5. Nanotube SR confirmed the threshold SR predictions for additive white Gaussian noise. The detector performance exhibited SR for four combinations of gate voltages and for three measures: the inverted bit error rate $1-\text{BER}$ (top blue), correlation measure $C(S,Y)$ (middle green), and mutual information $I(S,Y)$ (bottom red).

and (b) and about 0.01 for (c) and (d). Fig. 2(a) enlarges Fig. 5(c) and shows the SR effect for additive white Gaussian noise and for the subthreshold signal pair ON $= -1.6$ V and OFF $= -1.4$ V. The SR mode of the mutual-information curve is six times the value at minimal noise. The SR mode of the correlation-measure curve is three times the value at minimal noise. The SR mode of the inverted bit-error-rate curve shows a 40% improvement over the value at minimal noise.

We also passed impulsive or infinite-variance white noise through the nanotube detector to test whether it was robust to occasional large noise spikes. We chose the highly impulsive Cauchy noise [1], [9] for this task. This infinite-variance noise had the probability density function

$$p(n) = \frac{1}{\pi}\left(\frac{\gamma}{n^2+\gamma^2}\right) \tag{12}$$

for zero location and finite dispersion γ. Not all Cauchy experiments produced a measurable SR effect: Fig. 7(a) shows that a diminished SR effect still persists for Cauchy noise with subthreshold signal pair ON $= -2.0$ V and OFF $= -1.8$ V. The plot in 7(a) shows the SR effect with more than one mode. The large SR mode lies at dispersion $\gamma \approx 0.003$. A second SR mode lies at dispersion $\gamma \in (0.3, 0.4)$. The plots in 7(b) and 7(c) show an approximate SR effect for the SR mode at dispersion $\gamma = 0.05$ in 7(b) and $\gamma \approx 0.02$ in 7(c).

Some of the SR plots show more than one mode. Several researchers reported multimodal SR [93]–[95] in the plot of system performance against noise. The apparent multiple SR modes in the uniform experiments may be due to fluctuations. But the clear second mode for the Cauchy experiments may involve clipping: the limited dynamic range $[-5, 5]$ V of the data acquisition equipment may have produced the second peak in the graph as a truncation artifact because it clipped large spikes when it converted the infinite-variance Cauchy noise to voltage.

Plotting the input–output sequences S and Y also shows the SR effect. Fig. 8 shows three pairs of sample input and output se-

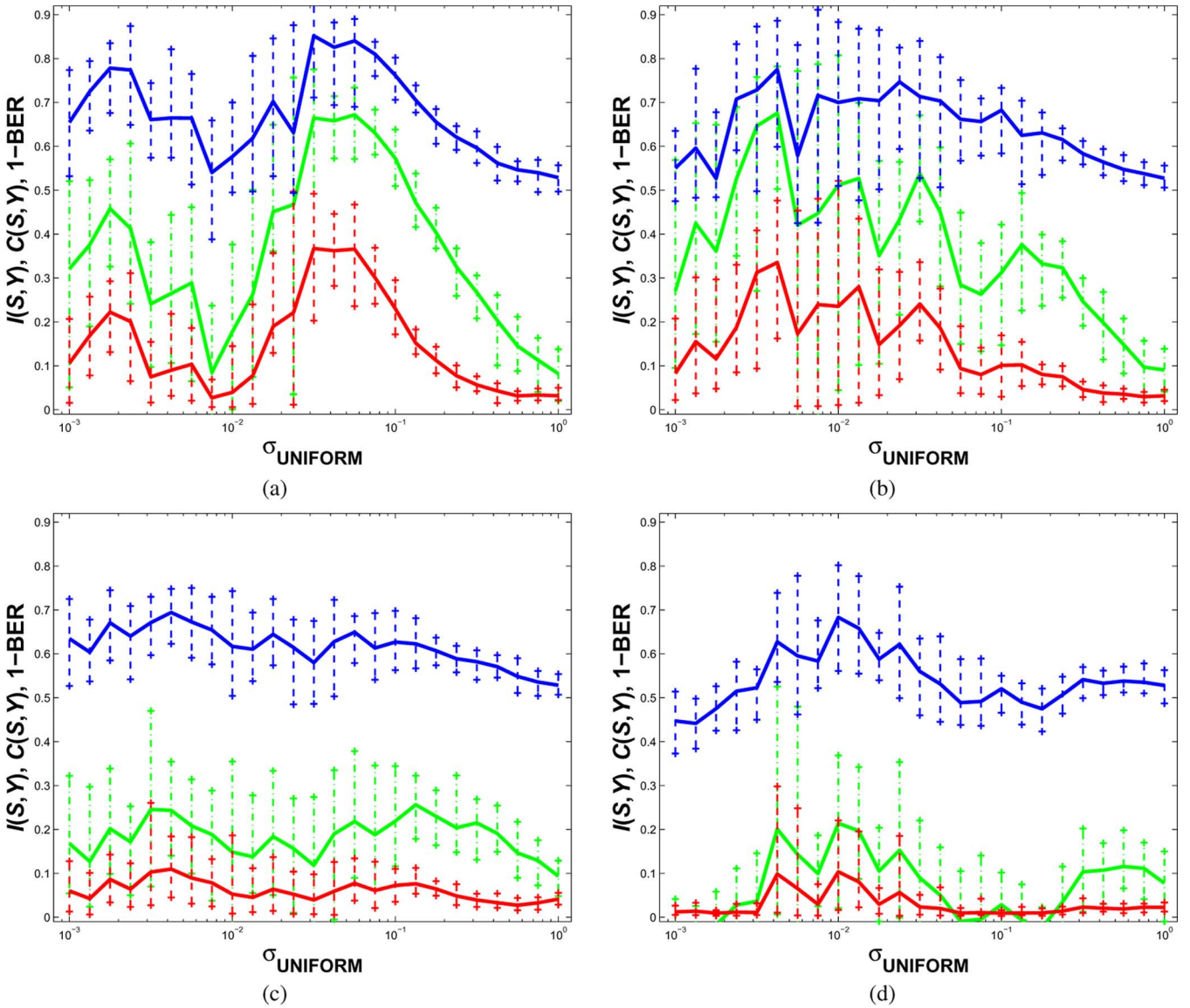

Fig. 6. Nanotube SR confirmed the threshold SR predictions for additive white uniform noise. The SR effect occurred for four combinations of gate voltages and for three performance measures: top blue for the inverted bit error rate, middle green for the input–output correlation, and bottom red for the mutual information. Two of the four plots appear to have multimodal SR curves.

quences. The top row shows the random binary (Bernoulli) input where the symbol $+1$ stands for ON and -1 for OFF. The bottom row shows the detector output for three different Gaussian noise standard deviations. A segment of the output sequence matches the input sequence better for near-optimal noise levels in Fig. 8(b) than for too little noise in 8(a) or too much in 8(c).

The experiments measured the detector's performance with the mutual information, the normalized correlation measure, and the inverted bit error rate. They measured how well the output sequence matched the input. The performance measures were discrete-time functions. Shannon's mutual information used probability densities of the input and the output sequences. A histogram of the output sequence Y gave the discrete probability density function

$$P(Y = Y_i) = p_i \tag{13}$$

that computed the unconditional Shannon entropy $H(Y) = -\sum_{i=1}^{N} p_i \ln p_i$ for mutual information without converting the detector output into a binary sequence with a threshold scheme. The histogram applied 120 equal-sized bins to the output sequence. Sorting the output sequence based on the binary input symbols and then applying the histogram gave the conditional output discrete probability density function

$$P_{Y|S}(Y = Y_i|S = S_j) = \frac{p_{ji}}{p_j} \tag{14}$$

conditioned on the input symbols that computed the conditional entropy $H(Y|S) = -\sum_{i=1}^{N}\sum_{j=1}^{N} p_{ji} \ln(p_{ji}/p_j)$. The mutual information measure was the difference between the unconditional and the conditional output entropies (9).

The correlation measure was the scalar inner product of the input and output sequences. A cross-correlation sequence compared the input and output symbol sequences and gave a measure of their match for different lag values l

$$r_{SY}(l) = \sum_{k=1}^{N} s(k)y(k-l) \tag{15}$$

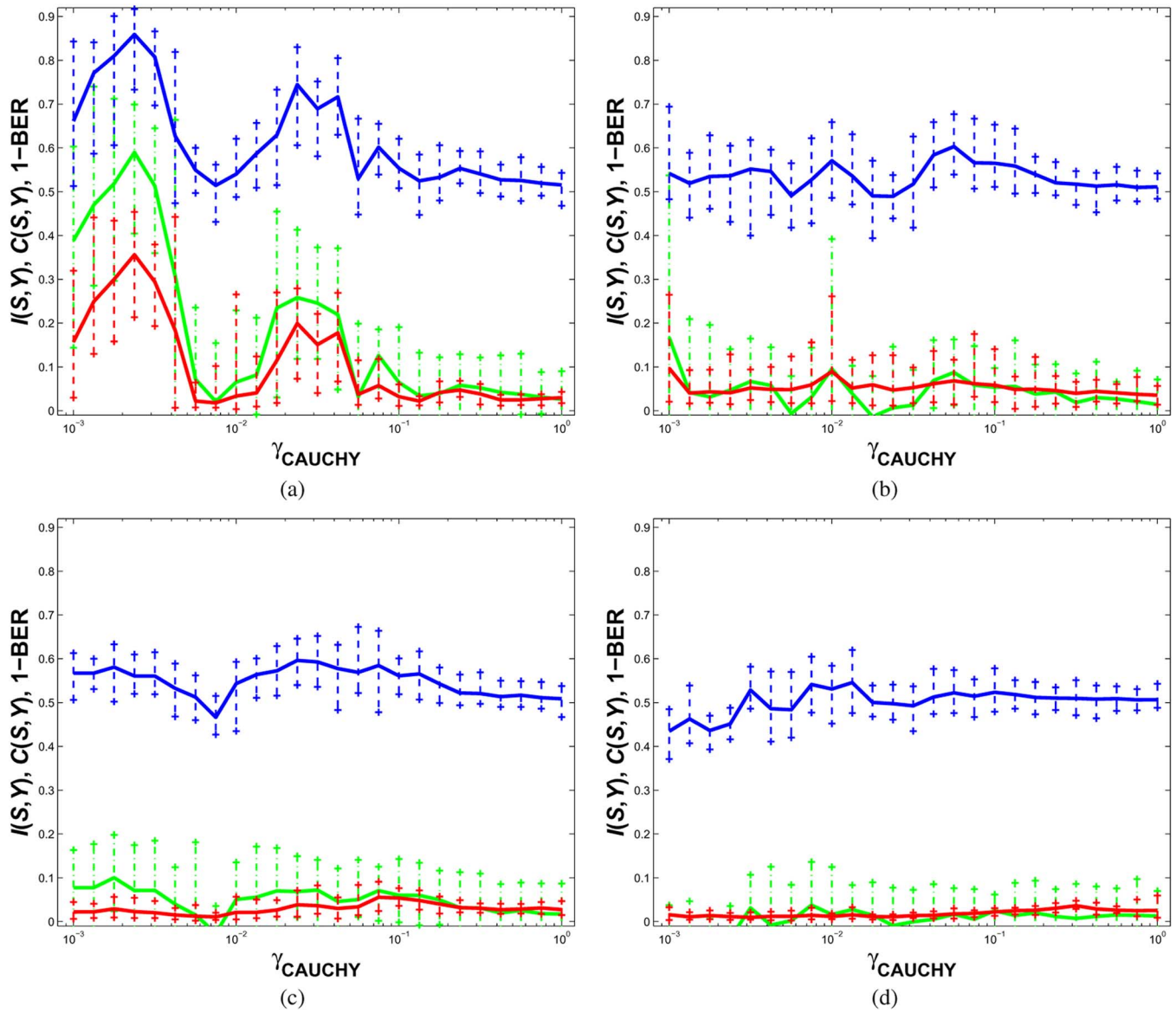

Fig. 7. Robust SR confirmed the threshold SR predictions for impulsive additive white Cauchy noise. The Cauchy-noise experiments produced a measurable SR effect for at least one combination of gate voltages and for three performance measures: the bottom red mutual information, the middle green cross correlation, and the top blue inverted bit error rate. The plot in (a) shows a clear SR effect with more than one mode.

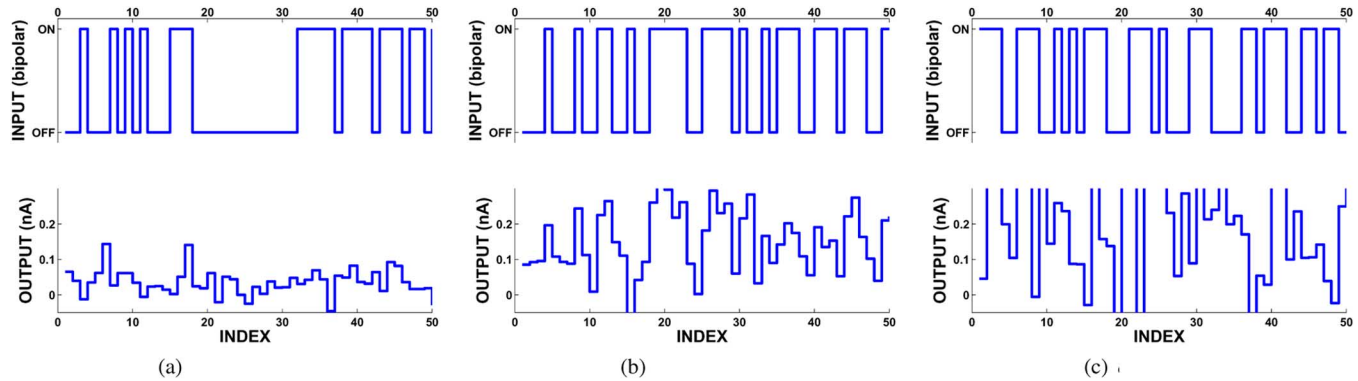

Fig. 8. Bernoulli input (top row) and detector output (bottom row) show the stochastic-resonance effect for additive white Gaussian noise. Three column-wise pairs of input and output sequences are: (a) dissimilar for small noise standard deviation $\sigma = 0.001$; (b) similar for optimal noise $\sigma_{\text{opt}} = 0.01$; and (c) dissimilar for large noise $\sigma = 1.0$. The output exceeds the scale in plot (c).

where the capital letters S and Y denoted the length-N random sequences and the lowercase letters $s(k)$ and $y(k)$ denoted values at some index k. The zero-lag ($l = 0$) value of the cross-correlation sequence (15) gave the scalar performance

measure that compared the input and output random sequences. Subtracting the sample mean from the output sequence improved the match between similar input and output sequences. The input Bernoulli sequence was approximately zero mean. The computation used $+1$ for the equally likely ON symbol and -1 for OFF so equal numbers of $+1$'s and -1's gave exactly zero mean. A normalization scheme divided the zero-lag cross correlation $r_{SY}(0)$ in (1) by the square root of the energy of the input and output sequences and gave the normalized correlation measure [19], [109]:

$$C(S,Y) = \frac{r_{SY}(0)}{\sqrt{|S|}\sqrt{|Y|}} = \frac{\sum_{k=1}^{N} s(k)y(k)}{\sqrt{\sum_{k=1}^{N} s(k)s(k)}\sqrt{\sum_{k=1}^{N} y(k)y(k)}} \quad (16)$$

where the energy of a sequence is the same as the zero-lag value of its autocorrelation

$$|x| = \sum_{k=1}^{N} x^2(k) = \sum_{k=1}^{N} x(k)x(k-l)|_{l=0} = r_{XX}(0). \quad (17)$$

The bit error rate measures how often a received bit or detector output y_i differs from the transmitted bit or input s_i. The experiments used complete information of the transmitted signal s_i and computed a threshold or discriminant function to classify the received bit y_i. Sorting by the input bit divided the output sequence into two clusters, one for each input binary symbol. Optimal two-class discrimination [23] used the midpoint between the cluster means for each sampled noise standard deviation σ (dispersion γ for Cauchy noise)

$$g(\sigma) = \frac{1}{2}\left[\frac{1}{N_{\mathrm{ON}}}\sum_{i=1}^{N_{\mathrm{ON}}}(y_i|s_i = \mathrm{ON}) + \frac{1}{N_{\mathrm{OFF}}}\sum_{i=1}^{N_{\mathrm{OFF}}}(y_i|s_i = \mathrm{OFF})\right]. \quad (18)$$

The threshold scheme converted an output Y to a binary sequence

$$Y_{\mathrm{binary}}(y_i, g) = \begin{cases} 1 & \text{for } y_i \geq g \\ 0 & \text{for } y_i < g \end{cases} \quad (19)$$

to compute the frequency of mismatch between the input and output binary sequences: $\mathrm{BER} = N_{\mathrm{error}}/N$ where N_{error} is the number of mismatching bits in a length-N sequence.

An increase in the bit-error-rate measure (BER) denotes a decrease in performance. So we inverted the BER by subtracting it from unity: $1 - \mathrm{BER} = N_{\mathrm{correct}}/N$ by counting the number of matching bits N_{correct} and created a convex (cup down) SR curve. We note that the BER measure has values in the range [0,0.5] and that the $1 - \mathrm{BER}$ measure has values in the range [0.5,1]. The apparent offset is due to the threshold detection of binary signals with two equally likely and subthreshold symbols. Both subthreshold symbols appear as OFF or 0 to the nanotube detector. So the maximal value of the BER measure (or $1 - \mathrm{BER}$) denotes that half of the subthreshold symbols is wrong (or correct).

The experiments applied discrete-time white noise of three types: Gaussian, uniform, and infinite-variance Cauchy noise. Fig. 9 shows samples of the three noise types in the left column (a), (d), and (g), their histograms in the center column (b), (e), and (h), and their power spectra in the right column (c), (f), and (i). The histogram estimates the discrete probability density function (pdf) of the noise. The bell-shaped curve in Fig. 9(e) and the flat line in Fig. 9(b) reflect the Gaussian and the uniform probability densities. Cauchy bell curves have fatter tails than do Gaussian bell curves: the impulsive Cauchy noise produces outliers more frequently. Clipping large values to ± 5 removed the occasional large spikes and produced the two peaks on either side of the Cauchy bell curve in Fig. 9(h). The power spectral density of the discrete-time zero-mean noise $n(k)$ is the discrete-time Fourier transformation of its autocorrelation sequence $R_n(e^{j\omega}) = \sum_{l=-\infty}^{\infty} r_n(l)\, e^{-j\omega l}$ where the autocorrelation sequence is $r_n(l) = \sum_{k=-\infty}^{\infty} n(k)\, n(k-l)$ [110].

The noise was white because the noise samples were uncorrelated in time. So the noise power spectrum was 2π-periodic and flat over the interval $[0, 2\pi]$ or equivalently $[-\pi, \pi]$. The lab equipment converted the Gaussian, the uniform, and the Cauchy noise samples to electrical voltages but clipped some Cauchy noise samples. The data acquisition equipment produced voltages in the interval $[-10, 10]$ V that a voltage divider reduced to the interval $[-5, 5]$ V. The voltage divider improved the voltage resolution for small noise values. The clipping had no effect for small dispersion values of up to 0.01.

Two new hypothesis tests verified that the SR curves were nonmonotonic and confirmed the nanotube SR effect. A χ^2-test and a Kolmogorov–Smirnov test both rejected the similarity between a monotonically decreasing β-probability density function and each of the three SR curves with p-value < 0.001. The statistical tests were goodness-of-fit tests that treated the SR curves as candidate pdfs and compared them against the benchmark β pdf (see Appendix).

Nanotube FET technology produced detectors that could exhibit hysteresis [18], [111], [112] or react to adsorbed molecules [113]–[115]. The detector was not ideal because its conductance, gate effect, and hysteresis changed over time. The detector exhibited some hysteresis but not enough to prevent the SR effect. A current–voltage I-V_G curve showed the hysteretic loop in Fig. 4. The HP 4156B stepped up the gate voltage V_G from -7.5 to 7.5 V and then stepped down to -7.5 V in a double sweep. The threshold voltage and the transconductance changed with a direction change of the gate voltage sweep. Charge trapping by water molecules on the silicon dioxide surface could cause hysteresis [18]. Researchers have reduced hysteresis by coating the nanotube devices with a layer of PMMA polymer and heating the coated devices [18].

The experimental design prevented the nonideal detector properties from confounding the results. The experiments treated the hysteretic nanotube detector as a *memoryless* discrete-time threshold instead of a bistable dynamical device such as the optical bistable system in [116]. The vacuum reduced the nanotube hysteretic effect but some effect persisted even after 72 h in vacuum. The subthreshold symbols were at least two

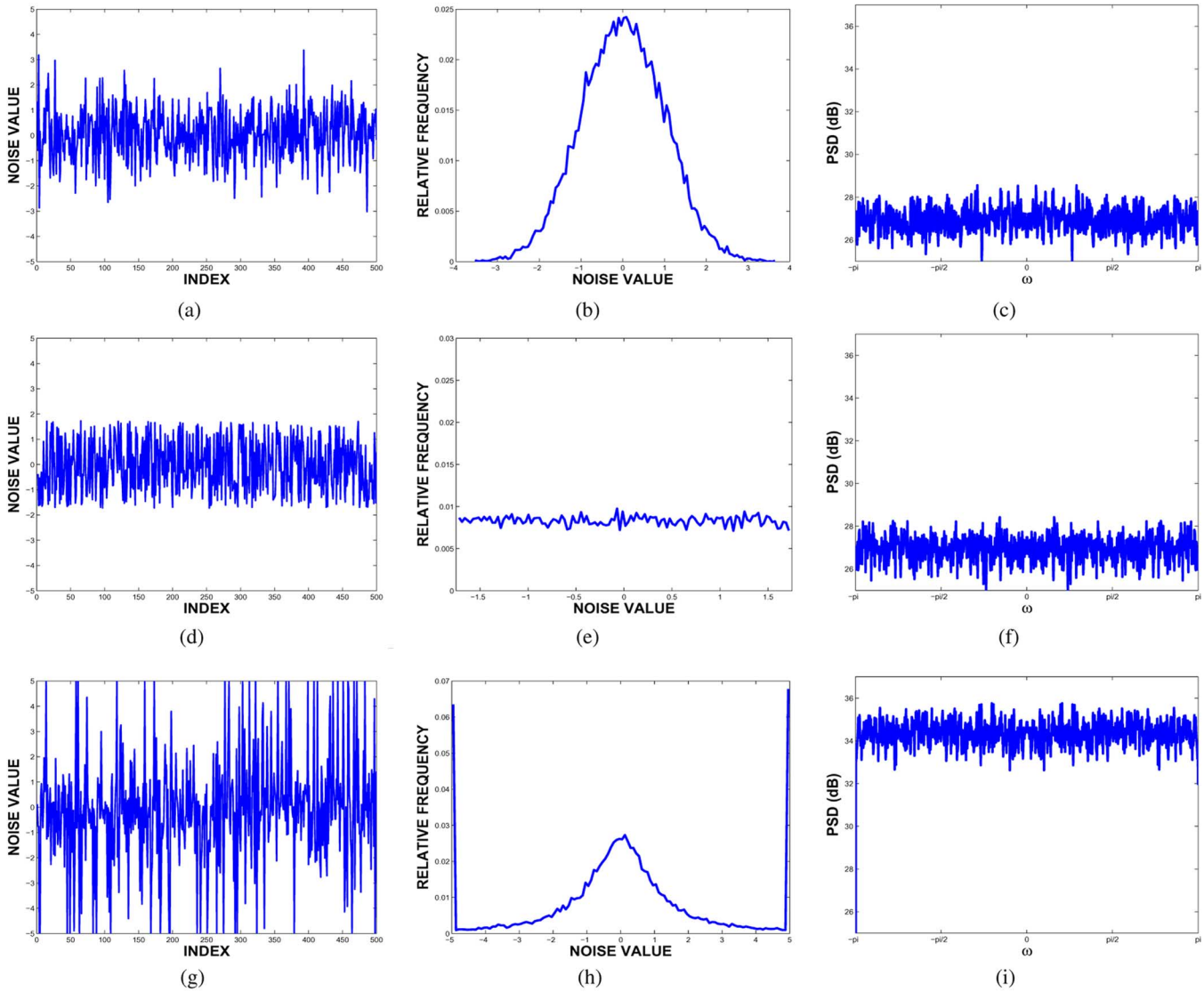

Fig. 9. Additive white (a) Gaussian, (d) uniform, and (g) clipped Cauchy noise samples. The noise samples had unit standard deviation $\sigma = 1.0$ ($\gamma = 1.0$ for Cauchy). (b), (e), and (h) show the histograms of the noise samples and estimate the discrete probability density function of the noise. (c), (f), and (i) show the discrete noise power spectral density.

standard deviations away from the far left leg of the hysteretic loop. Plotting the detector's random output Y as a function of its noisy input S gave a *stochastic* I-V_G curve that showed the nonideal but threshold-like gate effect of a transistor in Fig. 2(b). The input signals had shorter hold times, smaller voltage ranges, and faster voltage transitions than the *deterministic* voltage sweeps that gave the I-V_G curve in Fig. 3(b) and the hysteretic curves in Fig. 4. Again the hysteresis did not prevent the observation of the SR effect.

Control experiments verified that the SR effect occurred for the nanotube. They had no nanotube bridging the source and drain electrodes and applied only additive Gaussian noise. The nanotube-free devices had no gate effect: they gave subnano amp current for any gate voltage. These devices did not exhibit SR.

V. Conclusion

Nanotube experiments confirmed the specific prediction in [9] that threshold systems could exhibit the SR effect for finite-variance noise and infinite-variance noise: noise helped a carbon nanotube transistor detect subthreshold digital voltage signals. Two finite-variance noise types and one infinite-variance noise type enhanced the detection. Control experiments ensured that the SR effect depended on the nanotube detector. The nanotube experiments used multiple trials that varied the choices of parameters and used long sequences of random signals to test the nanotube detection. Three different measures showed the noise-enhanced detection and correlated well with one another. The statistical tests in the Appendix confirmed that the nanotube produced the signature SR humps in all three measures.

The experiments confirmed the SR prediction by testing a carbon nanotube transistor instead of a general class of nanoscale devices due to many limitations. Multiple experiments that used different nanotube devices should confirm our SR results but for the limited supply. The carbon nanotubes were fragile devices and many samples broke down during preparation. We designed the experiments to prevent unstable

device properties such as hysteresis from confounding the SR results and so treated the nanotubes as threshold devices. The nanotubes could have been bistable devices that detected continuous-time periodic signals in noise if they had stable hysteretic properties. Experiments on such nanotubes should exhibit a different type of SR such as in [116] because the detectors would be bistable. The transistor's backgate [26] produced parasitic capacitance that limited how fast the test signals could change. This prevented treating the nanotubes as high speed transistors [117] for communications or for high-speed integrated circuits [118]. Such applications should exhibit SR if the detectors have little parasitic capacitance. Arrays of nanotube threshold detectors [119] should also exhibit array SR effects [19]. Experiments on CMOS-like [120] nanotube inverters should also exhibit the SR effect and suggest nanotube applications in digital logic [121]. Experiments on transistors based on inorganic nanotubes [32] or semiconductor nanowires [33] should yield the same SR effects for nanotubes because they would satisfy the same threshold condition as did our carbon nanotube transistors.

The SR results in detection suggest that nanotubes can exploit noise in other signal processing tasks. The nanotube detectors should apply to broadband [106] or optical communications [122], [123] that use the submicroamp currents and the attenuated digital signals similar to our experiments. Nanotube transistors should apply to optical communications because they can change their conductivity in the presence of light [124] and can generate light [125]. Conducting nanotubes should apply to wireless communications because they can act as antennas [126] and use their lengths to code for specific frequencies by matching their impedances [127]. Researchers can grow nanotubes up to 2 mm [24] and design the lengths for a wide range of gigahertz frequencies. The nanotube SR effect should enhance receiver sensitivity because noise helped the nanotubes detect subthreshold digital signals that are similar to faint direct-sequence signals in spread spectrum communications [128].

Cell phone base stations sometimes implement frequency hopping spread spectrum with a bank of transmitters and receivers to cover a wide range of frequencies [129]. A very wide band receiver can use an array of nanotube detectors as the antenna array where each detector codes for a different narrowband frequency channel. A control signal can synchronize the search for data signals to a known frequency-hop sequence by turning on part of the detector array for a specific frequency at a specific time. Nanotubes should be able to detect a frequency-hop sequence by processing the signals in the bank of frequency-matched detectors much as a matched filter maximizes the signal to noise power ratio by setting its filter coefficients to a scaled replica of the known signal [110].

Nanotubes should also assist parallel processing [16] for a large number of elements in a small space because the nanotube transistors can be very small [130]. Researchers predict that the smallest nanotube transistor can have a conduction channel of length $l \approx 5$ nm and diameter $d \in [0.4, 2]$ nm. Chemical interactions could field-program arrays of nanotube electrical signal detectors to match a given signal level or to use existing noise to approximate the SR-optimal noise. Chemical additives can tune a nanotube array's sensitivity to electrical signals because adsorbed molecules change nanotube conductivity [113]–[115] and tune detector parameters such as their threshold voltages. Sensitivity analysis showed that the SR-optimal noise changed with the difference between the threshold voltage and the subthreshold signal level.

The nanotube detectors can implement pulse-train neural networks or interface with biological systems [131]. The detectors can implement pulse-train neural networks because they are threshold-like and similar to threshold and spiking neurons [132]. The nanotubes should detect model neural spike trains if the spike trains are Bernoulli sequences as in our experiments. The nanotube detectors should also detect biological neural impulses because nanotubes can operate in a biological environment such as a saline solution [133] and use the electrolyte as their gate [133], [134]. Field-reprogrammed nanotube detectors might also help exploit noise in model or biological [46], [55], [83], [135] systems if they can use the existing noise as the SR-optimal noise.

APPENDIX
SR HYPOTHESIS TESTS

Two statistical tests confirmed that the SR curves were nonmonotonic. A goodness-of-fit test measures how well a candidate probability density function (pdf) matches a benchmark pdf given a set of data from the candidate pdf. The null hypothesis H_0 states that the two pdfs are the same. The test rejects the null hypothesis if a test statistic exceeds a critical value for a given significance level α. The significance level α denotes the probability of a Type-I error—the probability of rejecting the null hypothesis when it is true. The p-value measures the credibility of the null hypothesis H_0 given the data. A statistical test rejects the null hypothesis H_0 at the significance level α if the p-value is less than the significance level: reject H_0 if p-value $< \alpha$. The popular β-pdf family has two shape parameters (α and θ) that give continuous pdfs over a finite-length interval such as the unit interval [1]. Some of these β-pdf decrease monotonically. These include the β-pdf in Fig. 10(a) with parameters $\alpha = 0.5$ and $\theta = 5$ among many others that we tested. Two types of goodness-of-fit tests rejected the match between the candidate (normalized) SR curves and the monotonically decreasing β-pdf $\sim \beta(0.5, 5)$. A β-pdf has the form

$$f_{\alpha,\theta}(x) = \frac{x^{\alpha-1}(1-x)^{\theta-1}}{B(\alpha,\theta)} \tag{20}$$

for $x \in [0, 1]$ and positive parameters $\alpha > 0$ and $\theta > 0$. The denominator term $B(\alpha, \theta)$ is

$$B(\alpha,\theta) = \int_0^1 x^{\alpha-1}(1-x)^{\theta-1}dx = \frac{\Gamma(\alpha)\Gamma(\theta)}{\Gamma(\alpha+\theta)} \tag{21}$$

with Γ function

$$\Gamma(n+1) = \int_0^\infty u^n e^{-u}du = n\Gamma(n) \tag{22}$$

for $n > 0$ ($\Gamma(1) = 1$ and $\Gamma(n+1) = n!$ if n is a positive integer). The β-pdf contrasts with the SR curves because it is nonzero

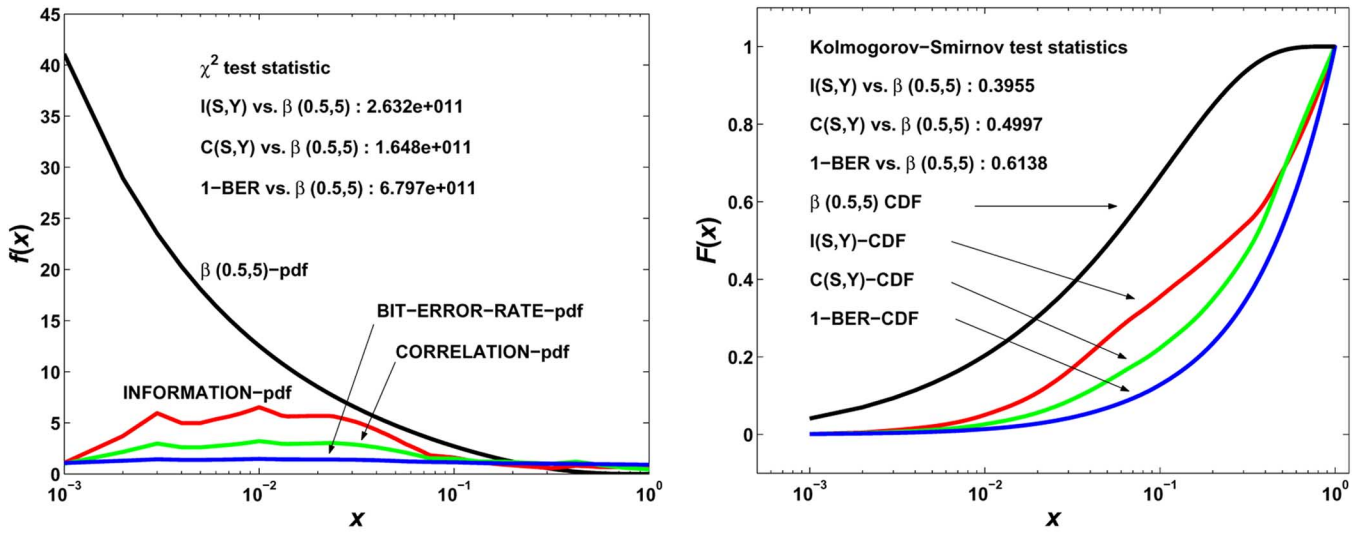

(a) (b)

Fig. 10. Tests of SR nonmonotonicity. Statistical tests compared the normalized stochastic-resonance (SR) curves and a monotonically decreasing β-probability density function (pdf). (a) The β-pdf (black curve) and the SR-pdfs (red for information, green for correlation, and blue for $1 - \text{BER}$). The reference-pdf curve had a β distribution ($\sim \beta(0.5, 5)$). (b) The beta-cumulative distribution function (CDF) and the SR-CDFs. Integrating the pdfs gave the CDFs.

only for $x \in [0, 1]$ and because it decreases monotonically to zero as x increases to 1 for the parameters $\alpha = 0.5$ and $\theta = 5$.

The goodness-of-fit tests converted each averaged SR curve to its equivalent pdf $f_{\text{SR}}(k)$. The conversion interpolated 25 averaged values so that the SR curves had a uniform increment of $\Delta x = 0.001$ and were nonzero only in the interval [1]. The conversion integrated (via discrete approximation) and normalized the SR curves so that they integrated to one

$$\int_{-\infty}^{\infty} f_{\text{SR}}(x)dx = \int_{0}^{1} f_{\text{SR}}(x)dx \approx \sum_{k=1}^{N} f_{\text{SR}}(k)\Delta x = 1 \quad (23)$$

where f_{SR} is the normalized SR curve.

The χ^2-test compared the SR-pdfs (mutual information, correlation measure, and inverted bit error rate) to the β-pdf in Fig. 10(a). We converted the pdf $f(k)$ to the cumulative distribution function (CDF) $F(k)$ by integration (via discrete approximation)

$$F(x) = \int_{-\infty}^{x} f(u)du = \int_{0}^{x} f(u)du \approx \sum_{j=1}^{k} f(j)\Delta x = F(k). \quad (24)$$

The CDF appeared in both a χ^2-test and a Kolmogorov–Smirnov (KS) test. The tests compared the SR-generated CDFs to the β-CDF in Fig. 10(b).

The goodness-of-fit test applied the χ^2-test with the null hypothesis H_0: SR-pdfs $\sim \beta(0.5, 5)$ and the alternate hypothesis H_a: SR-pdfs $\nsim \beta(0.5, 5)$ at the smallest level of significance $\alpha = 0.001$. The test rejected the null hypothesis if the test statistic exceeded the critical value. The test statistic had the form

$$\chi^2_{\text{test}} = \sum_{i} \frac{(O_i - E_i)^2}{E_i} \quad (25)$$

where O_i was an observed value in the SR-pdfs and E_i was an expected value in the reference β-pdf. The critical value was $\chi^2_{\text{critical}} = 48.2679$ for the smallest level of significance $\alpha = 0.001$ and for degree of freedom $\nu = (k - 1 - m) = (25 - 1 - 2) = 22$ where k was the number of data and m was the number of parameters in the test. The test statistic was $\chi^2_{\text{pdftest}} = 2.632 \times 10^{11}$ for the mutual-information pdf, $\chi^2_{\text{pdftest}} = 1.648 \times 10^{11}$ for the correlation-measure pdf, and $\chi^2_{\text{pdftest}} = 6.797 \times 10^{11}$ for the inverted bit-error-rate pdf. So the χ^2-test showed that the monotonically decreasing β-pdf differed substantially from any of the SR-pdfs with p-value < 0.001.

A second χ^2-test based on the CDF removed a potential confounding factor in the pdf-based test: the small values in the tail of the pdf might skew the test statistic if it gave near-zero values in its denominator. The CDF-based goodness-of-fit test applied the null hypothesis H_0: SR-CDFs $\sim \beta$ (0.5, 5) and the alternate hypothesis H_a: SR-CDFs $\nsim \beta$ (0.5, 5). The test statistic was $\chi^2_{\text{CDFtest}} = 89.2559$ for the mutual information CDF, $\chi^2_{\text{CDFtest}} = 129.1207$ for the correlation measure CDF, and $\chi^2_{\text{CDFtest}} = 212.8394$ for the inverted bit-error-rate CDF. The test statistics greatly exceeded the critical value $\chi^2_{\text{critical}} = 48.2679$. The χ^2-test showed that the β-CDF differed substantially from the SR-CDFs with p-value < 0.001.

The Kolmogorov–Smirnov (KS) test for goodness-of-fit also tested how well the SR-CDFs matched a β-CDF for the null hypothesis H_0: SR-CDFs $\sim \beta(0.5, 5)$ and the alternate hypothesis H_a: SR-CDFs $\nsim \beta(0.5, 5)$ by comparing the CDF-based test statistic to the critical value $\text{KS}_{\text{critical}} = 0.32$ for the smallest significance level $\alpha = 0.01$ and for $n = 25$ (number of data). The test statistic equaled the largest difference between the observed and the expected CDF values

$$\text{KS}_{\text{test}} = \max_{i}(|O_i - E_i|) \quad (26)$$

where O_i was an observed value in the SR-CDF and E_i was an expected value in the reference β-CDF. All three test statistics exceeded the critical value: $\text{KS}_{\text{test}} = 0.3955$ for the mutual-information CDF, $\text{KS}_{\text{test}} = 0.4997$ for the correlation-measure CDF, and $\text{KS}_{\text{test}} = 0.6138$ for the bit-error-rate CDF.

So the KS test rejected the null hypothesis and showed that the monotonic decreasing β-CDF differed from the SR-CDFs with p-value < 0.001.

ACKNOWLEDGMENT

The authors would like to thank C. Li, S. Mitaim, and A. Patel for helpful discussions.

REFERENCES

[1] B. Kosko and S. Mitaim, "Stochastic resonance in noisy threshold neurons," *Neural Netw.*, vol. 16, pp. 755–761, 2003.

[2] ——, "Adaptive stochastic resonance for noisy threshold neurons based on mutual information," in *IEEE Proc. Int. Joint Conf. Neural Networks (IJCNN'02)*, vol. 2, pp. 1980–1985.

[3] M. E. Inchiosa, J. W. C. Robinson, and A. R. Bulsara, "Information-theoretic stochastic resonance in noise-floor limited systems: The case for adding noise," *Phys. Rev. Lett.*, vol. 85, pp. 3369–3372, 2000.

[4] L. Gammaitoni and A. R. Bulsara, "Noise activated nonlinear dynamic sensors," *Phys. Rev. Lett.*, vol. 88, pp. 230 601-1–230 601-4, 2002.

[5] A. R. Bulsara and L. Gammaitoni, "Tuning in to noise," *Phys. Today*, pp. 39–45, Mar. 1996.

[6] Z. Gingl, L. Kiss, and F. Moss, "Non-dynamical stochastic resonance: Theory and experiments with white and arbitrarily coloured noises," *Europhys. Lett.*, vol. 29, pp. 191–196, 1995.

[7] K. Wiesenfeld and F. Moss, "Stochastic resonance and the benefits of noise: From ice ages to crayfish and SQUID's," *Nature*, vol. 373, pp. 33–36, Jan. 1995.

[8] F. Moss, D. Pierson, and D. O'Gorman, "Stochastic resonance: Tutorial and update," *Int. J. Bifurc. Chaos*, vol. 6, pp. 1383–1397, 1994.

[9] B. Kosko and S. Mitaim, "Robust stochastic resonance: Signal detection and adaptation in impulsive noise," *Phys. Rev. E*, vol. 64, pp. 051 110-1–051 110-11, Nov. 2001.

[10] X. Pei, L. Wilkens, and F. Moss, "Noise-mediated spike timing precision from aperiodic stimuli in an array of Hodgkin-Huxley type neurons," *Phys. Rev. Lett.*, vol. 77, no. 22, pp. 4679–4682, Nov. 1996.

[11] X. Pei, K. Bachmann, and F. Moss, "The detection threshold, noise and stochastic resonance in the Fitzhugh-Nagumo neuron model," *Phys. Lett. A*, vol. 206, pp. 61–65, Oct. 1995.

[12] S. J. Tans, R. M. Verschueren, and C. Dekker, "Room temperature transistor based on a single carbon nanotube," *Nature*, vol. 393, pp. 49–52, 1998.

[13] C. Zhou, J. Kong, and H. Dai, "Transport measurements of individual semiconducting singled-walled carbon nanotubes of various diameters," *Appl. Phys. Lett.*, vol. 76, p. 1597, 2000.

[14] R. Martel, T. Schmidt, H. R. Shea, T. Hertel, and P. Avouris, "Single and multi-wall carbon nanotube field-effect transistors," *Appl. Phys. Lett.*, vol. 73, pp. 2447–2449, 1998.

[15] C. L. Cheung, A. Kurtz, H. Park, and C. M. Lieber, "Diameter controlled synthesis of carbon nanotubes," *J. Phys. Chem. B*, vol. 106, pp. 2429–2429, 2002.

[16] J. L. Liu *et al.*, "Fullerene pipes," *Science*, vol. 280, pp. 1253–1256, 1998.

[17] R. Saito, M. Fujita, G. Dresselhaus, and M. S. Dresselhaus, "Electronic structure of chiral graphene tubules," *Appl. Phys. Lett.*, vol. 60, pp. 2204–2206, 1992.

[18] W. Kim *et al.*, "Hysteresis caused by water molecules in carbon nanotube field-effect transistors," *Nano Lett.*, vol. 3, pp. 193–198, 2003.

[19] N. G. Stocks, "Information transmission in parallel threshold arrays: Suprathreshold stochastic resonance," *Phys. Rev. E*, vol. 63, pp. 041 114–041 122, 2001.

[20] J. J. Collins, C. C. Chow, A. C. Capela, and T. T. Imhoff, "Aperiodic stochastic resonance," *Phys. Rev. E*, vol. 54, pp. 5575–5584, 1996.

[21] J. J. Collins, C. C. Chow, and T. T. Imhoff, "Aperiodic stochastic resonance in excitable systems," *Phys. Rev. E*, vol. 52, no. 4, pp. R3321–R3324, Oct. 1995.

[22] T. M. Cover and J. A. Thomas, *Elements of Information Theory*. New York: Wiley, 1991.

[23] R. O. Duda and P. E. Hart, *Pattern Classification and Scene Analysis*. New York: Wiley, 1973.

[24] S. Huang, X. Cai, and J. Liu, "Growth of millimeter-long and horizontally aligned single-walled carbon nanotubes on flat substrates," *J. Amer. Chem. Soc.*, vol. 125, no. 19, pp. 5636–5637, 2003.

[25] T. W. Ebbesen and P. M. Ajayan, "Large-scale synthesis of carbon nanotubes," *Nature*, vol. 358, p. 220, 1992.

[26] J. Kong, H. Soh, A. Cassell, C. F. Quate, and H. Dai, "Synthesis of individual single-walled carbon nanotubes on patterned silicon wafers," *Nature*, vol. 395, pp. 878–881, 1998.

[27] J. Hafner, M. Bronikowski, B. Azamian, P. Nikolaev, D. Colbert, and R. Smalley, "Catalytic growth of single wall carbon nanotubes from metal particles," *Chem. Phys. Lett.*, vol. 296, pp. 195–202, 1998.

[28] J. W. G. Wildoer, L. C. Venema, A. G. Rinzler, R. E. Smalley, and C. Dekker, "Electronic structure of atomically resolved carbon nanotubes," *Nature*, vol. 391, pp. 59–62, 1998.

[29] R. D. Antonov and A. T. Johnson, "Subband population in a single-wall carbon nanotube diode," *Phys. Rev. Lett.*, vol. 83, pp. 3274–3276, 1999.

[30] Z. Yao, H. W. C. Postma, L. Balents, and C. Dekker, "Carbon nanotube intramolecular junctions," *Nature*, vol. 402, pp. 273–276, 1999.

[31] X. Duan, C. Niu, V. Sahi, J. Chen, J. W. Parce, S. Empedocles, and J. L. Goldman, "High-performance thin-film transistors using semiconductor nanowires and nanoribbons," *Nature*, vol. 425, no. 6955, pp. 274–278, Sep. 2003.

[32] J. Goldberger, R. He, Y. Zhang, S. Lee, H. Yan, H.-J. Choi, and P. Yang, "Single-crystal gallium nitride nanotubes," *Nature*, vol. 422, pp. 599–602, Apr. 2003.

[33] M. Radosavljevi, J. Appenzeller, V. Derycke, R. Martel, P. Avouris, A. Loiseau, J.-L. Cochon, and D. Pigache, "Electrical properties and transport in boron nitride nanotubes," *Appl. Phys. Lett.*, vol. 82, pp. 4131–4133, Jun. 2003.

[34] X. Duan, Y. Huang, Y. Cui, J. Wang, and C. M. Lieber, "Indium phosphide nanowires as building blocks for nanoscale electronic and optoelectronic devices," *Nature*, vol. 409, pp. 66–69, Jan. 2001.

[35] L. Rotkina, J.-F. Lin, and J. P. Bird, "Nonlinear current–voltage characteristics of Pt nanowires and nanowire transistors fabricated by electron-beam deposition," *Appl. Phys. Lett.*, vol. 83, pp. 4426–4428, Nov. 2003.

[36] C. Li, B. Lei, D. Zhang, X. Liu, S. Han, T. Tang, M. Rouhanizadeh, T. Hsiai, and C. Zhou, "Chemical gating of In_2O_3 nanowires by organic and biomolecules," *Appl. Phys. Lett.*, vol. 83, pp. 4014–4016, Nov. 2003.

[37] D. Wang, Q. Wang, A. Javey, R. Tu, H. Dai, H. Kim, P. C. McIntyre, T. Krishnamohan, and K. C. Saraswat, "Germanium nanowire field-effect transistors with SiO2 and high- HfO2 gate dielectrics," *Appl. Phys. Lett.*, vol. 83, pp. 2432–2434, Sep. 2003.

[38] J.-R. Kim, H. M. So, J. W. Park, J.-J. Kim, J. Kim, C. J. Lee, and S. C. Lyu, "Electrical transport properties of individual gallium nitride nanowires synthesized by chemical-vapor-deposition," *Appl. Phys. Lett.*, vol. 80, pp. 3548–3550, May 2002.

[39] N. J. Pinto, A. T. Johnson, Jr, A. G. MacDiarmid, C. H. Mueller, N. Theofylaktos, D. C. Robinson, and F. A. Miranda, "Electrospun polyaniline/polyethylene oxide nanofiber field-effect transistor," *Appl. Phys. Lett.*, vol. 83, pp. 4244–4246, Nov. 2003.

[40] G. T. Kim, J. Muster, V. Krstic, J. G. Park, Y. W. Park, S. Roth, and M. Burghard, "Field-effect transistor made of individual V_2O_5 nanofibers," *Appl. Phys. Lett.*, vol. 76, pp. 1875–1877, Apr. 2000.

[41] C. Thelander, T. Mårtensson, M. T. Björk, B. J. Ohlsson, M. W. Larsson, L. R. Wallenberg, and L. Samuelson, "Single-electron transistors in heterostructure nanowires," *Appl. Phys. Lett.*, vol. 83, pp. 2052–2054, Sep. 2003.

[42] H. Namatsu, Y. Watanabe, K. Yamazaki, T. Yamaguchi, M. Nagase, Y. Ono, A. Fujiwara, and S. Horiguchi, "Fabrication of Si single-electron transistors with precise dimensions by electron-beam nanolithography," *J. Vac. Sci. Technol. B, Microelectron. Nanometer Struct.*, vol. 21, no. 1, pp. 1–5, Jan. 2003.

[43] R. Benzi, G. Parisi, A. Sutera, and A. Vulpiani, "Stochastic resonance in climatic change," *Tellus*, vol. 34, pp. 10–16, 1982.

[44] ——, "A theory of stochastic resonance in climatic change," *SIAM J. Appl. Math.*, vol. 43, no. 3, pp. 565–578, Jun. 1983.

[45] R. Benzi, A. Sutera, and A. Vulpiani, "The mechanism of stochastic resonance," *J. Phys. A, Math. Gen.*, vol. 14, pp. L453–L457, 1981.

[46] E. Pantazelou, C. Dames, F. Moss, J. Douglass, and L. Wilkens, "Temperature dependence and the role of internal noise in signal transduction efficiency of crayfish mechanoreceptors," *Int. J. Bifurc. Chaos*, vol. 5, no. 1, pp. 101–108, 1995.

[47] X. Pei, L. Wilkens, and F. Moss, "Light enhances hydrodynamic signaling in the multimodal caudal photoreceptor interneurons of the crayfish," *J. Neurophysiol.*, vol. 76, no. 5, pp. 3002–3011, Nov. 1996.

[48] J. K. Douglass, L. Wilkens, E. Pantazelou, and F. Moss, "Noise enhancement of information transfer in crayfish mechanoreceptors by stochastic resonance," *Nature*, vol. 365, pp. 337–340, 1993.

[49] J. E. Levin and J. P. Miller, "Broadband neural encoding in the cricket cercal sensory system enhanced by stochastic resonance," *Nature*, vol. 380, pp. 165–168, 1996.

[50] J. P. Miller, G. A. Jacobs, and F. E. Theunissen, "Representation of sensory information in the cricket cercal sensory system. I. Response properties of the primary interneurons," *J. Neurophysiol.*, vol. 66, no. 5, pp. 1680–1689, Nov. 1991.

[51] ——, "Representation of sensory information in the cricket cercal sensory system. II. Information theoretic calculation of system accuracy and optimal tuning-curve widths of four primary interneurons," *J. Neurophysiol.*, vol. 66, no. 5, pp. 1690–1703, Nov. 1991.

[52] H. A. Braun, H. Wissing, K. Schäfer, and M. C. Hirsch, "Oscillation and noise determine signal transduction in shark multimodal sensory cells," *Nature*, vol. 367, pp. 270–273, Jan. 1994.

[53] D. F. Russel, L. A. Wilkens, and F. Moss, "Use of behavioural stochastic resonance by paddlefish for feeding," *Nature*, vol. 402, pp. 291–294, 1999.

[54] B. J. Gluckman, T. I. Netoff, E. J. Neel, W. L. Ditto, M. L. Spano, and S. J. Schiff, "Stochastic resonance in a neuronal network from mammalian brain," *Phys. Rev. Lett.*, vol. 77, no. 19, pp. 4098–4101, Nov. 1996.

[55] J. J. Collins, T. T. Imhoff, and P. Grigg, "Noise-enhanced information transmission in rat SA1 cutaneous mechanoreceptors via aperiodic stochastic resonance," *J. Neurophysiol.*, vol. 76, pp. 642–645, 1996.

[56] B. McNamara, K. Wiesenfeld, and R. Roy, "Observation of stochastic resonance in a ring laser," *Phys. Rev. Lett.*, vol. 60, pp. 2626–2629, 1988.

[57] G. Vemuri and R. Roy, "Stochastic resonance in a bistable ring laser," *Phys. Rev. A*, vol. 39, no. 9, pp. 4668–4674, May 1989.

[58] V. S. Anishchenko, M. A. Safonova, and L. O. Chua, "Stochastic resonance in Chua's circuit," *Int. J. Bifurc. Chaos*, vol. 2, no. 2, pp. 397–401, 1992.

[59] ——, "Stochastic resonance in Chua's circuit driven by amplitude or frequency modulated signals," *Int. J. Bifurc. Chaos*, vol. 4, no. 2, pp. 441–446, 1994.

[60] X. Godivier and F. Chapeau-Blondeau, "Noise-assisted signal transmission in a nonlinear electronic comparator: Experiment and theory," *Signal Process.*, vol. 56, pp. 293–303, 1997.

[61] M. Löcher, G. A. Johnson, and E. R. Hunt, "Spatiotemporal stochastic resonance in a system of coupled diode resonators," *Phys. Rev. Lett.*, vol. 77, no. 23, pp. 4698–4701, Dec. 1996.

[62] R. N. Mantegna and B. Spagnolo, "Stochastic resonance in a tunnel diode," *Phys. Rev. E*, vol. 49, no. 3, pp. R1792–R1795, Mar. 1994.

[63] ——, "Stochastic resonance in a tunnel diode in the presence of white or colored noise," *Il Nuovo Cimento, Luglio-Agosto*, vol. 17 D, no. 7-8, pp. 873–881, 1995.

[64] V. I. Melnikov, "Schmitt trigger: A solvable model of stochastic resonance," *Phys. Rev. E*, vol. 48, no. 4, pp. 2481–2489, Oct. 1993.

[65] Z. N'eda, "Stochastic resonance in Ising systems," *Phys. Rev. E*, vol. 51, no. 6, pp. 5315–5317, Jun. 1995.

[66] S. W. Sides, R. A. Ramos, P. A. Rikvol, and M. A. Novotny, "Kinetic Ising system in an oscillating external field: Stochastic resonance and residence-time distributions," *J. Appl. Phys.*, vol. 81, no. 8, pp. 5597–5599, Apr. 1997.

[67] J. J. Brey and A. Prados, "Stochastic resonance in a one dimension Ising model," *Phys. Lett. A*, vol. 216, pp. 240–246, Jun. 1996.

[68] L. Gammaitoni, M. Martinelli, L. Pardi, and S. Santucci, "Observation of stochastic resonance in bistable electro-paramagnetic-resonance systems," *Phys. Rev. Lett.*, vol. 67, no. 13, pp. 1799–1802, Sep. 1991.

[69] A. N. Grigorenko and P. I. Nikitin, "Stochastic resonance in a bistable magnetic system," *IEEE Trans. Magn.*, vol. 31, no. 5, pp. 2491–2493, Sep. 1995.

[70] M. L. Spano, M. Wun-Fogle, and W. L. Ditto, "Experimental observation of stochastic resonance in a magnetoelastic ribbon," *Phys. Rev. A*, vol. 46, no. 8, pp. 5253–5256, Oct. 1992.

[71] R. Rouse, S. Han, and J. E. Lukens, "Flux amplification using stochastic superconducting quantum interference devices," *Appl. Phys. Lett.*, vol. 66, no. 1, pp. 108–110, Jan. 1995.

[72] A. Hibbs, E. W. Jacobs, J. Bekkedahl, A. R. Bulsara, and F. Moss, "Signal enhancement in a r.f. SQUID using stochastic resonance," *Il Nuovo Cimento, Luglio-Agosto*, vol. 17 D, no. s. 7-8, pp. 811–817, 1995.

[73] A. D. Hibbs, A. L. Singsaas, E. W. Jacobs, A. R. Bulsara, J. J. Bekkedahl, and F. Moss, "Stochastic resonance in a superconducting loop with Josephson junction," *J. Appl. Phys.*, vol. 77, no. 6, pp. 2582–2590, Mar. 1995.

[74] P. Bryant, K. Wiesenfeld, and B. McNamara, "The nonlinear effects of noise on parametric amplification: An analysis of noise rise in Josephson junctions and other systems," *J. Appl. Phys.*, vol. 62, pp. 2898–2913, 1987.

[75] R. Bartussek, P. Hänggi, and P. Jung, "Stochastic resonance in optical bistable systems," *Phys. Rev. E*, vol. 49, no. 5, pp. 3930–3939, May 1994.

[76] M. I. Dykman, G. P. Golubev, I. K. Kaufman, D. G. Luchinsky, P. V. E. McClintock, and E. A. Zhukov, "Noise-enhanced optical heterodyning in an all-optical bistable system," *Appl. Phys. Lett.*, vol. 67, no. 3, pp. 308–310, Jul. 1995.

[77] M. I. Dykman, T. Horita, and J. Ross, "Statistical distribution and stochastic resonance in a periodically driven chemical system," *J. Chem. Phys.*, vol. 103, no. 3, pp. 966–972, Jul. 1995.

[78] H. A. Kramers, "Brownian motion in a field of force and the diffusion model of chemical reactions," *Physica*, vol. 7, no. 4, pp. 284–304, Apr. 1940.

[79] D. S. Leonard and L. E. Reichl, "Stochastic resonance in a chemical reaction," *Phys. Rev. E*, vol. 49, no. 2, pp. 1734–1737, Feb. 1994.

[80] A. Förster, M. Merget, and F. W. Schneider, "Stochastic resonance in chemistry 2: The peroxidase-oxidase reaction," *J. Phys. Chem.*, vol. 100, pp. 4442–4447, 1996.

[81] A. Guderian, G. Dechert, K.-P. Zeyer, and F. W. Schneider, "Stochastic resonance in chemistry. 1. The Belousov–Zhabitinsku reaction," *J. Phys. Chem.*, vol. 100, pp. 4437–4441, 1996.

[82] R. Löfstedt and S. N. Coppersmith, "Quantum stochastic resonance," *Phys. Rev. Lett.*, vol. 72, no. 13, pp. 1947–1950, Mar. 1994.

[83] D. E. Makarov and N. Makri, "Stochastic resonance and nonlinear response in double-quantum-well structures," *Phys. Rev. B*, vol. 52, no. 4, pp. R2257–R2260, Jul. 1995.

[84] T. P. Pareek, M. C. Mahato, A. M. M. Thorwart, and P. Jung, "Dynamical hysteresis in bistable quantum systems," *Phys. Rev. Lett.*, vol. 78, no. 13, pp. 2503–2506, Mar. 1997.

[85] Jayannavar, "Stochastic resonance and nonlinear response in a dissipative quantum two-state system," *Phys. Rev. B*, vol. 55, no. 15, pp. 9318–9321, Apr. 1997.

[86] M. Grifoni and P. Hänggi, "Nonlinear quantum stochastic resonance," *Phys. Rev. E*, vol. 54, no. 2, pp. 1390–1401, Aug. 1996.

[87] M. I. Dykman and P. V. E. McClintock, "Power spectra of noise driven nonlinear systems and stochastic resonance," *Physica D*, vol. 58, no. 10, pp. 10–30, 1992.

[88] A. R. Bulsara, R. D. Boss, and E. W. Jacobs, "Noise effects in an electronic model of a single neuron," *Biol. Cybern.*, vol. 61, pp. 211–222, 1989.

[89] M. I. Dykman, D. G. Luchinsky, R. Mannella, P. V. E. McClintock, S. M. Soskin, and N. D. Stein, "Resonant subharmonic absorption and second-harmonic generation by a fluctuating nonlinear oscillator," *Phys. Rev. E*, vol. 54, no. 3, pp. 2366–2377, Sep. 1996.

[90] M. I. Dykman, D. G. Luchinsky, R. Mannella, P. V. E. McClintock, N. D. Stein, and N. G. Stocks, "Nonconventional stochastic resonance," *J. Stat. Phys.*, vol. 70, no. 1/2, pp. 479–499, Jan. 1993.

[91] ——, "Supernarrow spectral peaks and high-frequency stochastic resonance in systems with coexisting periodic attractors," *Phys. Rev. E*, vol. 49, no. 2, pp. 1198–1215, Feb. 1994.

[92] S. M. Soskin and P. V. E. McClintock, "Comment on 'Monostable array-enhanced stochastic resonance'," *Phys. Rev. E*, vol. 66, pp. 013 101-1–013 101-3, 2002.

[93] J. F. Lindner, B. J. Breen, M. E. Wills, A. R. Bulsara, and W. L. Ditto, "Monostable array-enhanced stochastic resonance," *Phys. Rev. E*, vol. 63, pp. 051 107-1–051 107-6, 2001.

[94] S. Matyjaskiewicz, A. Krawiecki, J. A. Holyst, K. Kacperski, and W. Ebeling, "Stochastic multiresonance in a chaotic map with fractal basins of attraction," *Phys. Rev. E*, vol. 63, pp. 026 215-1–026 215-10, 2001.

[95] J. M. G. Vilar and J. M. Rubí, "Stochastic multiresonance," *Phys. Rev. Lett.*, vol. 78, pp. 2882–2885, 1997.

[96] A. R. Bulsara, E. W. Jacobs, T. Zhou, F. Moss, and L. Kiss, "Stochastic resonance in a single neuron model: Theory and analog simulation," *J. Theor. Biol.*, vol. 152, pp. 531–555, 1991.

[97] A. Longtin, "Autonomous stochastic resonance in bursting neurons," *Phys. Rev. E*, vol. 55, no. 1, pp. 868–876, Jan. 1997.

[98] R. Plonsey and R. C. Barr, *Bioelectricity: A Quantitative Approach*. New York: Plenum, 1988.

[99] A. Longtin, "Synchronization of the stochastic FitzHugh-Nagumo equations to periodic forcing," *IL Nuovo Cimento, Luglio- Agosto*, vol. 17D, no. 7–8, pp. 835–846, 1995.

[100] F. Moss, J. K. Douglass, L. Wilkens, D. Pierson, and E. Pantazelou, "Stochastic resonance in an electronic FitzHugh-Nagumo model," in *Stochastic Processes in Astrophysics*, J. R. Buchler and H. E. Krup, Eds. New York: Ann. NY Acad. Sci., 1993, vol. 706, pp. 26–41.

[101] D. Pierson, J. K. Douglass, E. Pantazelou, and F. Moss, P. H. Hanel and A. L. Chung, Eds., "Using an electronic FitzHugh–Nagumo simulator to mimic noisy electrophysiological data from stimulated crayfish mechanoreceptor cells," in *AIP Conf. Proc. 285 Noise in Physical Systems and 1/f Fluctuations*, 1993, pp. 731–734.
[102] A. R. Bulsara, T. C. Elston, C. R. Doering, S. B. Lowen, and K. Lindenberg, "Cooperative behavior in periodically driven noisy integrate-fire models of neuronal dynamics," *Phys. Rev. E*, vol. 53, no. 4, pp. 3958–3969, Apr. 1996.
[103] F. Chapeau-Blondeau and X. Godivier, "Stochastic resonance in nonlinear transmission of spike signals: An exact model and an application to the neuron," *Int. J. Bifurc. Chaos*, vol. 6, no. 11, pp. 2069–2076, 1996.
[104] H. E. Plesser and S. Tanaka, "Stochastic resonance in a model neuron with reset," *Phys. Lett. A*, vol. 225, pp. 228–234, Feb. 1997.
[105] M. Stemmler, "A single spike suffices: The simplest form of stochastic resonance in model neurons," *Netw. Comput. Neural Syst.*, vol. 7, pp. 687–716, 1996.
[106] A. R. Bulsara and A. Zador, "Threshold detection of wideband signals: A noise-induced maximum in the mutual information," *Phys. Rev. E*, vol. 54, pp. R2185–R2185, 1996.
[107] L. Gammaitoni, "Stochastic resonance in multi-threshold systems," *Phys. Lett. A*, vol. 208, pp. 315–322, Dec. 1995.
[108] X. Godivier and F. Chapeau-Blondeau, "Stochastic resonance in the information capacity of a nonlinear dynamic system," *Int. J. Bifurc. Chaos*, vol. 8, no. 3, pp. 581–589, 1998.
[109] A. V. Oppenheim, R. W. Schafer, and J. R. Buck, *Discrete-Time Signal Processing*, 2nd ed. Upper Saddle River, NJ: Prentice-Hall, 1999.
[110] V. K. Ingle, D. G. Manolakis, and S. Kogon, *Statistical and Adaptive Signal Processing: Spectral Estimation, Signal Modeling, Adaptive Filtering and Array Processing*. New York: McGraw-Hill, 1999.
[111] M. S. Fuhrer, B. M. Kim, T. Durkop, and T. Bringlinger, "High-mobility nanotube transistor memory," *Nano Lett.*, vol. 2, pp. 755–759, 2002.
[112] M. Radosavljevic, M. Freitag, K. V. Thadani, and A. T. Johnson, "Nonvolatile molecular memory elements based on ambipolar nanotube field effect transistors," *Nano Lett.*, vol. 2, pp. 761–764, 2002.
[113] K. G. Ong, K. Zeng, and C. A. Grimes, "A wireless, passive carbon nanotube-based gas sensor," *IEEE Sensors J.*, vol. 2, no. 2, pp. 82–88, Apr. 2002.
[114] P. G. Collins, K. Bradley, M. Ishigami, and A. Zettl, "Extreme oxygen sensitivity of electronic properties of carbon nanotubes," *Science*, vol. 287, pp. 1801–1804, 2000.
[115] J. Kong *et al.*, "Nanotube molecular wires as chemical sensors," *Science*, vol. 287, pp. 622–625, 2000.
[116] M. Misono, T. Kohmoto, M. Kunitomo, and Y. Fukuda, "Information gain in an optical bistable system by stochastic resonance," *Phys. Rev. E*, vol. 67, pp. 061 102–061 105, Jun. 2003.
[117] T. Dürkop, S. A. Getty, E. Cobas, and M. S. Fuhrer, "Extraordinary mobility in semiconducting carbon nanotubes," *Nano Lett.*, vol. 4, no. 1, pp. 35–39, 2004.
[118] D. Harris and M. A. Horowitz, "Skew-tolerant domino circuits," *IEEE J. Solid-State Circuits*, vol. 32, no. 11, pp. 1702–1711, Nov. 1997.
[119] Y.-C. Tseng, P. Xuan, A. Javey, R. Malloy, Q. Wang, J. Bokor, and H. Dai, "Monolithic integration of carbon nanotube devices with silicon MOS technology," *Nano Lett.*, vol. 4, no. 1, pp. 123–127, 2004.
[120] X. Liu, C. Lee, and C. Zhou, "Carbon nanotube field-effect inverters," *Appl. Phys. Lett.*, vol. 79, no. 20, pp. 3329–3331, Nov. 2001.
[121] A. Bachtold, P. Hadley, T. Nakanishi, and C. Dekker, "Logic circuits with carbon nanotube transistors," *Science*, vol. 294, pp. 1317–1317, 2001.
[122] S. Barbay, G. Giacomelli, and F. Marin, "Noise-assisted transmission of binary information: Theory and experiment," *Phys. Rev. E*, vol. 63, pp. 051 110–051 118, 2000.
[123] Y. C. Chen *et al.*, "Ultrafast optical switching properties of single-wall carbon nanotube polymer composites at 1.55 μm," *Appl. Phys. Lett.*, vol. 81, pp. 975–977, 2002.
[124] M. Shim and G. P. Siddons, "Photoinduced conductivity changes in carbon nanotube transistors," *Appl. Phys. Lett.*, vol. 83, no. 17, pp. 3564–3566, Oct. 2003.
[125] J. A. Misewich, R. Martel, P. Avouris, J. C. Tsang, S. Heinze, and J. Tersoff, "Electrically induced optical emission from a carbon nanotube FET," *Science*, vol. 300, no. 5620, pp. 783–786, May 2003.
[126] W. Liang, M. Bockrath, D. Bozovic, J. H. Hafner, M. Tinkham, and H. Park, "Fabry–Perot interference in a nanotube electron waveguide," *Nature*, vol. 411, pp. 665–669, 2001.
[127] L. V. Blake, "Open-circuited and short-circuited lines can also behave like resonant circuits. This behavior occurs when the length of the line is an integral multiple of a quarter wavelength," in *Antennas*. Dedham, MA: Artech House, 1984, pp. 69–70.
[128] R. Irmer and G. Fettweis, "Combined transmitter and receiver optimization for multiple-antenna frequency-selective channels," in *Proc. Wireless Personal Multimedia Communications (WPMC'02)*, pp. 412–416.
[129] M. K. Simon, J. K. Omura, R. A. Scholtz, and B. K. Levitt, *Spread Spectrum Communications Handbook*, rev. ed. New York: McGraw-Hill, 1994.
[130] A. Rochefort, M. D. Ventra, and P. Avouris, "Switching behavior of semiconducting carbon nanotubes under an external electric field," *Appl. Phys. Lett.*, vol. 78, pp. 2521–2523, 2001.
[131] T. J. Webster, M. C. Waid, J. L. McKenzie, R. L. Price, and J. U. Ejiofor, "Nano-biotechnology: Carbon nanofibres as improved neural and orthopaedic implants," *Nanotechnology*, vol. 15, pp. 48–54, Jan. 2004.
[132] F. Rieke, D. Warland, and R.d.R.v. Stevenick, *Spikes. Exploring the Neural Code*. Cambridge, MA: MIT Press , 1999.
[133] M. Kruger, M. R. Buitelaar, T. Nussbaumer, C. Schonenberger, and L. Forro, "Electrochemical carbon nanotube field-effect transistor," *Appl. Phys. Lett.*, vol. 78, pp. 1291–1293, 2001.
[134] P. L. McEuen, M. S. Fuhrer, and H. Park, "Single-walled carbon nanotube electronics," *IEEE Trans. Nanotechnol.*, vol. 1, no. 1, pp. 78–85, Mar. 2002.
[135] F. Jaramillo and K. Wiesenfeld, "Mechanoelectrical transduction assisted by Brownian motion: A role for noise in the auditory system," *Nature Neurosci.*, vol. 1, pp. 384–3884, 1998.

Ian Y. Lee received the Ph.D. degree in electrical engineering from the University of Southern California, Los Angeles.

His research interests include applications of fuzzy neural systems and biomedical engineering, nanosignal processing using nanotubes and nanowires, armor applications for nanomaterials, and stochastic resonance.

Xiaolei Liu is working toward the Ph.D. degree in the Department of Electrical Engineering—Electrophysics of the University of Southern California, Los Angeles.

His research interests include nanomaterial synthesis and characterization, nanoelectronics, mesoscopic physics, and molecular electronics.

Chongwu Zhou received the Ph.D. degree in electrical engineering from Yale University, New Haven, CT, in 1999.

He is an Assistant Professor at the Department of Electrical Engineering—Electrophysics of the University of Southern California, Los Angeles. He has published numerous book chapters and research papers. His research interests include nanomaterial synthesis and characterization, nanoelectronics and nanophotonics, mesoscopic physics, molecular electronics, and nanoscale biosensors.

Dr. Zhou has received a National Science Foundation CAREER Award and a NASA TGiR Award.

Bart Kosko (M'85) holds degrees in philosophy, economics, applied mathematics, electrical engineering, and law.

He is a Professor of Electrical Engineering at the University of Southern California (USC), Los Angeles, a past director of USC's Signal and Image Processing Institute, and has chaired and cochaired several neural and fuzzy conferences. He has published the textbooks *Neural Networks and Fuzzy Systems* and *Fuzzy Engineering*, the trade books *Fuzzy Thinking* and *Heaven in a Chip*, the novel *Nanotime*, edited the textbook *Neural Networks for Signal Processing*, and coedited the volume *Intelligent Signal Processing*. His most recent book is *Noise*.